Accepted Manuscript

Discovery and optimization of 1-(1*H*-indol-1-yl)ethanone derivatives as CBP/EP300 bromodomain inhibitors for the treatment of castration-resistant prostate cancer

Qiuping Xiang, Chao Wang, Yan Zhang, Xiaoqian Xue, Ming Song, Cheng Zhang, Chenchang Li, Chun Wu, Kuai Li, Xiaoyan Hui, Yulai Zhou, Jeff B. Smaill, Adam V. Patterson, Donghai Wu, Ke Ding, Yong Xu

PII: S0223-5234(18)30109-0

DOI: 10.1016/j.ejmech.2018.01.087

Reference: EJMECH 10164

To appear in: *European Journal of Medicinal Chemistry*

Received Date: 8 September 2017

Revised Date: 11 January 2018

Accepted Date: 26 January 2018

Please cite this article as: Q. Xiang, C. Wang, Y. Zhang, X. Xue, M. Song, C. Zhang, C. Li, C. Wu, K. Li, X. Hui, Y. Zhou, J.B. Smaill, A.V. Patterson, D. Wu, K. Ding, Y. Xu, Discovery and optimization of 1-(1*H*-indol-1-yl)ethanone derivatives as CBP/EP300 bromodomain inhibitors for the treatment of castration-resistant prostate cancer, *European Journal of Medicinal Chemistry* (2018), doi: 10.1016/j.ejmech.2018.01.087.

Graphical abstract

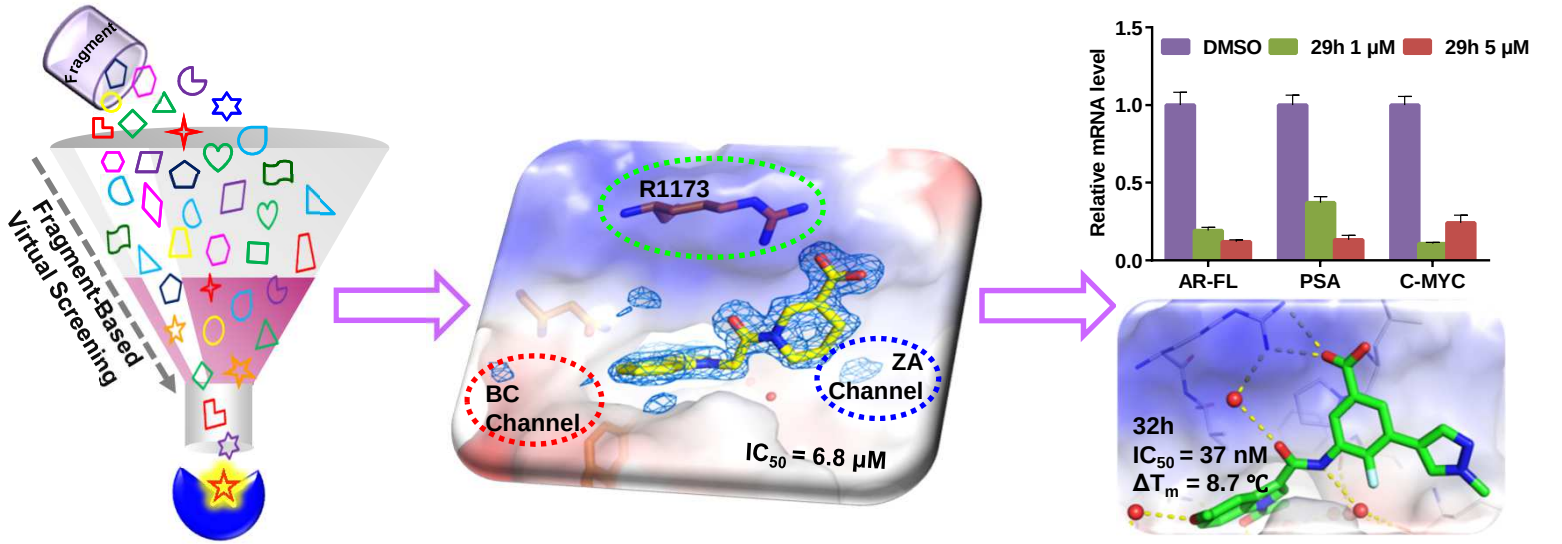

Structure Based Discovery

Co-crystal structure of 22e−CBP

CBP represents a potential target of PCa

Discovery and optimization of 1-(1*H*-indol-1-yl)ethanone derivatives as CBP/EP300 bromodomain inhibitors for the treatment of castration-resistant prostate cancer

Qiuping Xiang,[†,‡,#] Chao Wang,[†,§,#] Yan Zhang,[†,‡] Xiaoqian Xue,[†,‡] Ming Song,[†] Cheng Zhang,[†,§] Chenchang Li,[†,§] Chun Wu,[†] Kuai Li,[†] Xiaoyan Hui,[¶] Yulai Zhou,[§] Jeff B. Smaill,[⊥] Adam V. Patterson,[⊥] Donghai Wu,[†] Ke Ding,[▽] and Yong Xu[†,*]

[†]Guangdong Provincial Key Laboratory of Biocomputing, Joint School of Life Sciences, Guangzhou Institutes of Biomedicine and Health, Chinese Academy of Sciences; Guangzhou Medical University, Guangzhou, China.

[‡]University of Chinese Academy of Sciences, No. 19 Yuquan Road, Beijing 100049, China.

[§]School of Pharmaceutical Sciences, Jilin University, Changchun, China, No.1266 Fujin Road, Chaoyang District, Changchun, Jilin 130021, China.

[¶]State Key Laboratory of Pharmaceutical Biotechnology, Department of Medicine, The University of Hong Kong, Hong Kong SAR.

[⊥]University of Auckland, Auckland Cancer Society Research Centre, School of Medical Sciences, Private Bag 92019, Auckland, NZ.

[▽]School of Pharmacy, Jinan University, 601 Huangpu Avenue West, Guangzhou 510632, China.

[*]Corresponding Author: Yong Xu, PhD, E-mail: xu_yong@gibh.ac.cn

[#]These authors contributed equally to this work.

ABSTRACT:

The CREB (cAMP responsive element binding protein) binding protein (CBP) and its homolog EP300 have emerged as new therapeutic targets for the treatment of cancer and inflammatory diseases. Here we report the identification, optimization and evaluation of 1-(1*H*-indol-1-yl)ethanone derivatives as CBP/EP300 inhibitors starting from fragment-based virtual screening (FBVS). A cocrystal structure of the inhibitor (**22e**) in complex with CBP provides a solid structural basis for further optimization. The most potent compound **32h** binds to the CBP bromodomain and has an IC_{50} value of 0.037 μM in the AlphaScreen assay which was 2 times more potent than the reported CBP bromodomain inhibitor SGC-CBP30 in our hands. **32h** also exhibit high selectivity for CBP/EP300 over other bromodomain-containing proteins. Notably, the ester derivative (**29h**) of compound **32h** markedly inhibit cell growth in several prostate cancer cell lines including LNCaP, 22Rv1 and LNCaP derived C4-2B. Compound **29h** suppresses the mRNA expression of full length AR (AR-FL), AR target genes and other oncogene in LNCaP cells. **29h** also reduces the expression of PSA, the biomarker of prostate cancer. CBP/EP300 inhibitor **29h** represents a promising lead compound for the development of new therapeutics for the treatment of castration-resistant prostate cancer.

Key words:

CBP; Prostate cancer; Bromodomain inhibitor

Abbreviations

CBP, CREB binding protein; PCa, prostate cancer; CRPC, castration-resistant prostate cancer; AR, androgen receptor; BET, Bromodomain and extra terminal protein; FBVS, fragment-based virtual screening; SAR, structure-activity relationship; TSA, thermal stability shift assay

1. Introduction

Prostate cancer (PCa) is the most common malignancy in men and remains the second leading cause of cancer mortality in men [1,2]. Androgen-deprivation therapy (ADT) represents the gold standard treatment for PCa. Despite the initial benefit, the majority of patients will progress to an incurable stage known as castration-resistant prostate cancer (CRPC) within 2−3 years. CRPC remains androgen receptor (AR) signaling dependent and responds to the recently approved androgen-signaling inhibitor enzalutamide and the androgen-synthesis inhibitor abiraterone acetate. However, most patients eventually develop resistance to these second-generation therapies as well. Therefore, an alternative strategy for the development of new therapeutic agents is urgently needed. One potential strategy is to disrupt AR upstream and/or downstream signaling without directly targeting the AR ligand binding domain (LBD). Recently, Chinnaiyan and others have shown that bromodomain-containing protein 4 (BRD4) inhibitors could disrupt the interaction between the N-terminal domain (NTD) of AR and BRD4 and block metastatic CRPC growth in animal models [3-5]. Sadar and others have shown that EPI-001 covalently binds to the AR NTD, blocking the transcriptional activity of AR and its splice variants and reducing the growth of CRPC xenografts [6-8]. We have shown that retinoic acid receptor-related orphan receptor γ (RORγ) acts upstream of AR as a key determinant of AR gene expression and that the RORγ antagonist XY018 can potently inhibit the growth of various AR-positive xenograft tumors in mice [9,10].

CREB (cAMP responsive element binding protein) binding protein (CBP) and its homolog EP300 are two closely related transcriptional regulators bearing LXXLL motifs.

They act as steroid receptor co-activators for various nuclear receptors, including the retinoid X receptor (RXR), estrogen receptor (ER) and AR [11-15]. CBP and EP300 have been implicated in the development of various cancers, inflammatory conditions, and other diseases [16-23]. In the advanced prostate cancer, CBP is highly expressed, and its expression level has been found positively linked with cancer patient survival [24,25]. Mechanistically, CBP and EP300 interact with the AR NTD to potentially stabilize both N/C interactions and AR binding to AREs (AR response elements) [13]. Therefore, interrupting the CBP-AR NTD interaction through targeting the bromodomain of CBP may be an efficient strategy to block AR signaling, and the CBP bromodomain may represent a potential therapeutic target for prostate cancer.

There has been significant progress in the development of small molecule inhibitors targeting the CBP bromodomain [20,25-35]. Among these inhibitors, compounds **1** and **2** were reported by Zhou using NMR spectroscopy [25]. Compound **1** was discovered by screening a focused library of 200 compounds and was the first compound that was shown to inhibit the CBP-p53 interaction at 50 μM (Figure 1). Unzue and co-workers have developed acetyl benzene compound **3** (Figure 1) as an inhibitor of CBP by fragment-based docking and structure-guided optimization. Compound **3** showed moderate potency against CBP, with an IC_{50} of 8.7 μM as determined by TR-FRET [34]. Isoxazole derivatives were initially developed for targeting BET bromodomains and later optimized as CBP bromodomain inhibitor (**4**, SGC-CBP30, Figure 1) [20]. Recently, compound **5** (I-CBP112, Figure 1), with a 1,4-benzoxazepine scaffold, was reported as a

CBP chemical probe and displayed good selectivity for CBP over other bromodomains and good cellular activity [29].

These studies enhance our understanding of the role of CBP in oncology, which could potentially pave the way for the development of therapeutics for various diseases. However, more chemotypes are still urgently needed in order to exploit the therapeutic potential of CBP inhibition in different human diseases such as prostate cancer.

In the present study, we report the fragment-based virtual screening, structure-guided medicinal optimization and biological evaluation of 1-(1*H*-indol-1-yl)ethanone derivatives as potent and selective CBP/EP300 bromodomain inhibitors for the treatment of castration-resistant prostate cancer.

2. Results and discussion

2.1 Identification and validation of 1-(1*H*-indol-1-yl)ethanone and 1-(1*H*-indol-3-yl)ethanone scaffold.

To obtain new scaffold of CBP inhibitors, a common virtual screening strategy [10,36-38] was used as shown in Figure 2A. The SPECS database was first filtered with a molecular weight threshold of less than 300. After that, the resulting set of fragments was screened through molecular docking-based evaluation. After cluster analysis and visual inspection, 13 representative compounds were selected and purchased for biological evaluation. The inhibitory activity and structures of the 13 compounds were shown in Figure 2B, Supporting Information Table S1 and Figure S2. Using an AlphaScreen assay, 3 of the 13 compounds showed micromolar-level activity, with IC_{50} values less than 50 μM. Compounds **6** (3-(3-acetyl-1*H*-indol-1-yl)propanoic acid) and **7** (1-(4,6-dinitro-1*H*-indazol-1-yl)ethanone) showed IC_{50} values of 16.73, and 9.11 μM, respectively (Figure 2C). Not surprisingly, the **6** has a similar scaffold with the ligand of 4TS8. The corresponding ligand efficiencies were approximately 0.4. These two compounds bear different scaffolds and represent good starting points for further optimization. To further evaluate the selectivity, 3 more bromodomain-containing proteins, BRD4(1), BAZ2B, and ATAD2, were tested to assess the activity of these two fragments by the AlphaScreen assay. The result showed that **7** displayed equipotent activities for all the bromodomain-containing proteins tested. However, **6** showed excellent selectivity for the CBP bromodomain over other bromodomain-containing proteins (Table S2). This result prompted us to choose **6** as a starting point for optimization. To design more potent derivatives, we also compared the binding modes of

6 and **7** bound to CBP (Figure 3A,B). The predicted binding mode of **7** bound to CBP showed that **7** interacts with the conserved residues Asn1168 and Tyr1125 through direct and water-mediated hydrogen bonds (Figure 3B). The binding model of **6** is characterized by the presence of a hydrogen bond between the carbonyl group of the 1-(1*H*-indol-3-yl)ethanone ring and the Asn1168 side chain of CBP (Figure 3A). The carbonyl group also interacts with Tyr1125 through an indirect hydrogen bond via a conserved water molecule present in the ZA channel. In addition, the propionic acid group forms favorable hydrogen bonds with Arg1173. From the predicted binding mode analysis, we can see that the 1-(1*H*-indol-3-yl)ethanone moiety of **6** could serve as an acetylated lysine mimic and that three regions could be explored for further optimization of this lead compound (Figure 3A). The first area is the LPF shelf, the second area is the ZA channel, and the third area is the BC channel.

2.2 Chemistry.

The derivatives of 1-(1*H*-indol-1-yl)ethanone and 1-(1*H*-indol-3-yl)ethanone were designed and synthesized as shown in Schemes 1–3.

Briefly, intermediates **21a−21b** were prepared by acylation of secondary amines **20a−20b** followed by reaction with 1-(1*H*-indol-3-yl)ethanone to produce 1-(1*H*-indol-1-yl)ethanone derivatives **22b** and **22c** in good yields. Compounds **22d** and **22e** were obtained by hydrolysis of compounds **22b** and **22c**, respectively. Compound **22a** was readily synthesized using a procedure similar to the one used to prepare **22b**.

The synthesis of **25a−25e** is illustrated in Scheme 2. 1-acetyl-1*H*-indole-3-carboxylic acid (**24a**) was first prepared by acetylization of 1*H*-indole-3-carboxylic acid (**23a**) with acetic anhydride, followed by condensation with various amines to yield the desired products. The ester **25c** was hydrolyzed under basic conditions to yield the corresponding carboxylic acid (**26**), which was acetylated to afford compound **25e**.

Intermediates **27a−27l** were prepared according to Scheme 3. The corresponding carboxylic acids **30a−l** were prepared by deprotection of **27a−27l** with TFA. Compound **29a** was directly demethylated with BBr_3 to give **32b**, which was subsequently etherified to generate final products **32c** and **32d**.

Compounds **28a−28q** and **29a−29h** were prepared using the procedure outlined in Scheme 3, which is similar to the procedure used in the preparation of **27a−27l**. Compounds **31a−31q**, **32a** and **32e−32h** were prepared by a procedure similar to what was used for the synthesis of **30a−30l**. The synthesis of compounds **32b−32d** is also outlined in Scheme 3.

Scheme 1. Synthesis of 1-(1*H*-indol-3-yl)ethanone Derivatives 22a−22e[a]

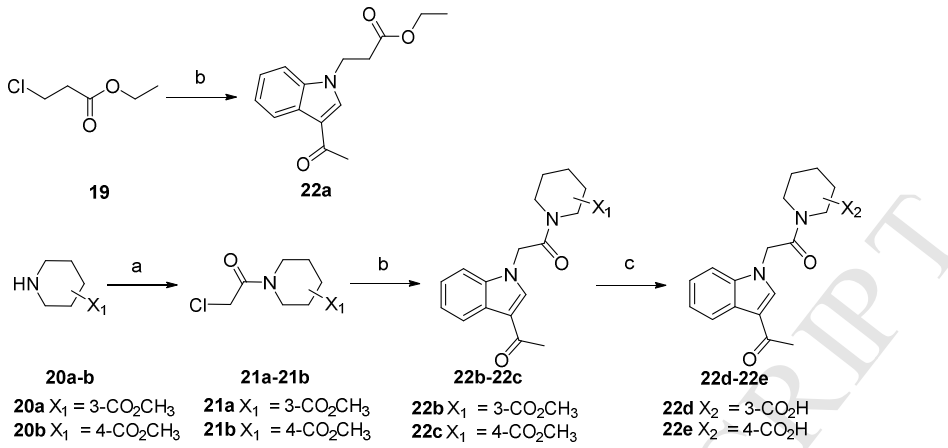

[a]Reagents and conditions: (a) acetic anhydride, K_2CO_3, DCM, 5 h, rt, 60−80%; (b) 1-(1*H*-indol-3-yl)ethanone, K_2CO_3, KI, 5 h, reflux, 70−80%; (c) NaOH, MeOH, rt, 2 h, 57−80%.

Scheme 2. Synthesis of 1-(1*H*-indol-1-yl)ethanone derivatives 25a−25e[a]

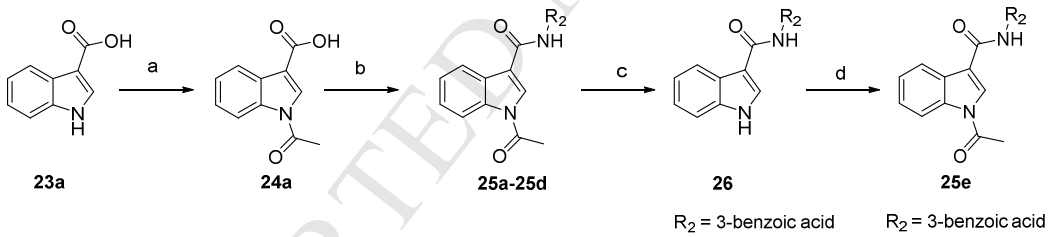

[a]Reagents and conditions: (a) acetic anhydride, Et_3N, DMAP, DCE, 2 h, 60 ºC, 38−63%; (b) aliphatic amines, HATU, DIPEA, DCM, overnight, rt, 60−71%; or aryl amines, n-Bu_3N, 2-chloro-1-methylpyridinium iodide, toluene, 16 h, 90 ºC, 30−68%; (c) NaOH, MeOH, overnight, rt, 83%; (d) Et_3N, DMAP, DCE, 12 h, 60 ºC, 35%.

Scheme 3. Synthesis of compounds 29a−29h, 30a−30l, 31a−31q, 32a−32h[a]

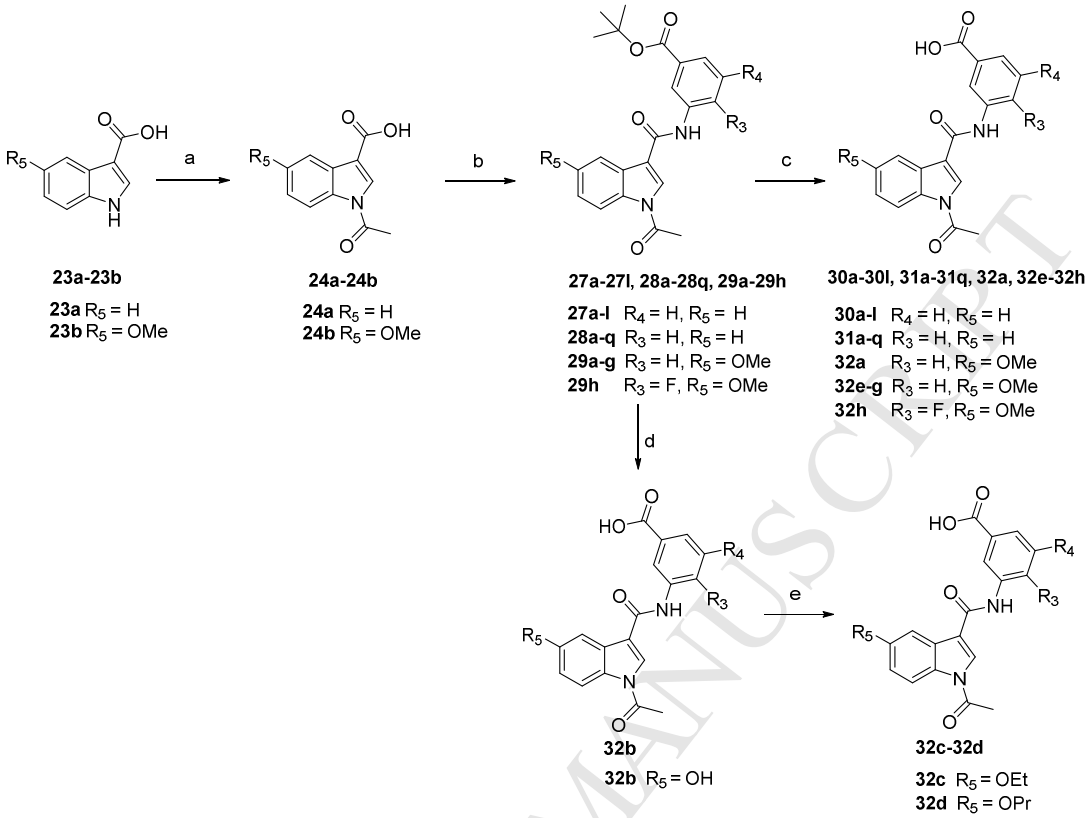

[a]Reagents and conditions: (a) acetic anhydride, Et_3N, DMAP, DCE, 2 h, 60 ºC, 38−63%; (b) aryl amines, n-Bu_3N, 2-chloro-1-methylpyridinium iodide, toluene, 16 h, 90 ºC, 35−68%; (c) TFA, DCM, 6 h, rt, 58−90%; (d) BBr_3, DCM, 15 h, rt, 60% (for reactant **29a**); (e) bromoethane or iodopropane, K_2CO_3, KI, acetone, 12 h, 70 ºC，38−43%.

2.3. Structure−activity relationship studies of the LPF shelf.

To discuss the structure−activity relationships of the LPF shelf, we designed various compounds with substituents on the head group, 1-(1*H*-indol-3-yl)ethanone. The binding affinities of these compounds to CBP were determined and summarized in Table 1. To ensure that these compounds can reach the LPF shelf and form further interactions with CBP, the propionic acid group originally present in **6** was replaced with larger groups. As shown in Table 1, replacing the propionic acid group in **6** with the corresponding ethyl

ester yielded **22a**, which was found to have a very weak binding affinity to CBP. Considering the flexibility of **22a**, we designed and synthesized conformational constrained analogs **22b**−**22e**. Compounds **22b** and **22d** exhibited potencies similar to **6**. **22c** and **22e** were 2-fold more potent than **6**, and they exhibited IC_{50} values of 7.09 and 6.80 μM, respectively. The results indicated that adding a substituent at the meta-position of the piperidine can improve ligand binding affinity.

To understand the structural basis for the protein-ligand interactions, we determined the cocrystal structure of the **22e**–CBP complex. As shown in Figure 4A and 4B, the binding mode of **22e** is clearly defined by the electron density map. **22e** plugs into the narrow pocket with its 1-(1*H*-indol-3-yl)ethanone group interacting with the conserved residues Asn1168 and Tyr1125. The 1-propionylpiperidine-3-carboxylic acid group can protrude out of the pocket and reach the LPF shelf, forming further interactions with CBP. The carboxyl group was involved in a canonical hydrogen bond with Arg1173. The crystal structure also revealed that the carbonyl of the 1-propionylpiperidine-3-carboxylic acid group interacts with Arg1173 through a water-mediated hydrogen bond. There are five water molecules located in the ZA channel. To obtain more potent compounds through water-mediated hydrogen bonds, the head group 1-(1*H*-indol-3-yl)ethanone was replaced with 1-(1*H*-indol-1-yl)ethanone with an amide linker attached.

We synthesized compounds **25a** and **25b**, which showed weaker affinities than **22e** (Table 1). It seems that the flexibility of the attached group may be detrimental to CBP affinity. Replacing the alkyl group with an aromatic group led to **25c**, which was found to bind to

CBP protein with an IC_{50} value of 3.39 μM and was twice as potent as **22e**. The corresponding acid form of **25c** was also synthesized (**25e**) and evaluated. Compound **25e** showed a small increase in activity with IC_{50} value of 1.69 μM, while the acetyl analog **25d** showed a sharp decrease in potency (IC_{50} = 25.37 μM) relative to compound **25e**. This finding demonstrated that the carboxyl group of **25e**, also seen in **22e**, was critical for compound activity.

Analysis of the predicted binding mode of compound **25e** in complex with the CBP bromodomain suggested that the NH group of the amide forms a new hydrogen bond with one of the conserved water molecule near the ZA channel. The phenyl group of **25e** extends to the LPF shelf and forms VDW interactions with the hydrophobic residue Leu1109. The carboxyl group of compound **25e** had the optimal orientation to form a very favorable hydrogen bond with the guanidinium group of Arg1173 of the CBP bromodomain (Figure 4C). It was indicated that a carboxyl group at the meta-position of phenyl ring was more favorable than other groups.

2.4. Structure−activity relationship studies of the ZA channel.

To investigate the SAR in the direction of the ZA channel, the preferred carboxyl group was maintained. The substitutions on the ortho- or meta-position (R_3 or R_4 in Table 2) were explored to improve the hydrophobic interactions with the ZA channel. First, short-chain alkyl groups were attached at the R_3 position and yielded **30a−30c**. Compound **30b**, with a longer-chain substitution, showed a significant loss of activity compared with the parent compound **25e**. The relatively small groups are well tolerated,

and the corresponding compounds showed activity similar to that of **25e**. When the hydrophobic cycloalkyl groups (**30d−30f**) were used to occupy the hydrophobic pocket, a small increase in inhibition was observed. Analogs **30e** and **30f** demonstrated IC_{50} values of 1.89 and 1.67 μM, respectively. To determine the importance of hydrophobic interactions, polar atoms were introduced to the cycloalkyl group. If the substituent atom is an O, as in **30g**, a 4-fold decrease in inhibition was observed. This result demonstrated that incorporation of a polar atom causes a reduction in the inhibitory activity. A flexible linker of one methylene carbon was used to attach polar substituents in hopes of improving activity (**30h−30k**). However, these compounds did not show improved activity. When a halogen atom (F) was introduced to the R_3-position, significantly improved potency was achieved; Compound **30l** was found to display an IC_{50} value of 0.77 μM. As shown in Figure 5A, the predicted binding mode of compound **30l** was similar to that of compound **25e**. The size of F atom is critical and may contribute to the improved activity. This finding suggested that small substituents at the R_3 position were favorable, while the larger groups may interfere with other residues around this pocket.

For the meta-position (R_4, Table 2), various substitutions were introduced to increase the binding affinity through improving close contact with the protein surface. The results are shown in Table 2. Compounds with alkyl or cycloalkyl groups did not improve the activity. Among these compounds, analog **31f** was one of the best compounds with moderate biochemical activity (IC_{50} = 2.48 μM). Flexible linkers with 1 or 2 atoms (**31g** and **31h**) were also used to attach polar substituents for improved activity. Not surprisingly, compound **31g** demonstrated high potency, with an IC_{50} value of 1.0 μM.

To find more potent analogs based on the modeled structure of **25e** in complex with CBP bromodomain, we designed compounds with various aromatic groups at the R_4 position to explore the chemical space for affinity improvement (Table 2). The phenyl ring analog (**31i**) showed similar potency to **25e** against CBP, with an IC_{50} value of 1.86 μM. The mono-substituted phenyl analogs were synthesized, leading to compounds **31j−31m**. No significant potency improvement was obtained. When a chlorine atom was substituted at the meta-position (**31k**), the activity matched that of **31e**.

To investigate the importance of polar atoms, we synthesized compounds **31n−31q**. **31n** exhibited a slightly increased potency compared to compound **31i**. Analog **31o** was one of the most promising compounds with strong biochemical activity (IC_{50} = 0.65 μM). Compound **31p** binds to CBP with IC_{50} value of 2.81 μM, which is one-fourth as strong as **31o**. This finding may be due to the hydrophobic phenyl group of compound **31p** being exposed to the solvent environment. Compound **31q** showed comparable activity, with an IC_{50} value of 1.00 μM. Analysis of the predicted binding mode for compound **31o** in complex with CBP protein (Figure 5B) suggested that the furan group orient along the ZA channel, increasing binding affinity through close contact with the protein surface. The O atom of the furan ring is exposed to the solvent environment, which is favorable for ligand binding. The results demonstrated that the furan group of **31o** is a favorable group in the ZA channel.

2.5. Structure−activity relationship studies of the BC channel.

Analysis of the predicted binding mode for compound **31o** in complex with CBP bromodomain showed that there is still some space near the BC channel for further optimization. As shown in Table 2, we designed various substituents at the R_5 position to explore the chemical space around the BC channel for affinity improvements. We synthesized compound **32b** with a hydroxy group at the R_5 position, which gave an IC_{50} value of 0.17 μM, making it 4 times more potent than **31o**. Expanding the size of alkoxy group, compounds **32a**, **32c** and **32d** were prepared to improve the activity. Compound **32a** showed activity (IC_{50} = 0.14 μM) similar to that of **32b**. However, compounds **32c** and **32d** have IC_{50} values of 3.89 and 26.19 μM, respectively. From the predicted binding mode, we can see that the substituent from this direction should also be exposed to solvent, so a larger alkyl group may decrease the potency. These results suggested that the optimal length of the substitution is approximately 1−2 heavy atoms. We next synthesized compounds **32e** and **32f**, which were found to bind to CBP with IC_{50} values of 0.29 and 0.69 μM, respectively. From the data shown in Table 2, we can see that heterocyclic substituents at the R_4 position are favorable. Changing the furan group in **32a** to a 1-methyl-1*H*-pyrazole led to **32g**, which showed an activity (IC_{50} = 0.16 μM) similar to that of **32a** (IC_{50} = 0.14 μM). The results demonstrated that the BC channel is also a critical region for potency (Figure 5B,C). Taken together, our modifications at the BC channel have yielded compounds **32a** and **32g** with much improved activities over the initial compounds **30l** and **31o**.

Combining all the substituents at R_3, R_4 and R_5 positions, we synthesized compound **32h**. **32h** demonstrated significantly improved activity with an IC_{50} of 0.037 μM, which was

approximately 4 times more potent than **32g** and 2 times more potent than compound **4** The phenyl group with fluorine, carbonyl, and 1-methyl-1*H*-pyrazole substituents fit snugly in the pocket as shown in Figure 5D. The hydrogen bonding and polar interactions may contribute to the improved potency.

2.6. Evaluation of bromodomains selectivity.

To investigate the selectivity profile, representative compounds were tested against 8 bromodomain-containing proteins from different subgroups of the bromodomain family using an AlphaScreen assay (Table 3). Most of the tested compounds showed excellent selectivity for the CBP bromodomain and its paralog EP300 over other bromodomain-containing proteins. Compounds **31o** and **32a** demonstrated high potency, with IC_{50} values of 0.65 and 0.14 μM for CBP, respectively; however, they also showed weak potency for some other bromodomain-containing proteins. Compounds **6**, **25e**, **30l**, and **31g** showed excellent selectivity. Among all the tested compounds, **32g** and **32h** showed best activity and selectivity profiles. To further confirm the selectivity over other bromodomain-containing proteins, compound **32g** and **32h** were evaluated against 8 bromodomain-containing proteins using a thermal stability shift (TSA) assay (Figure 6). Similar to the AlphaScreen assay, the TSA assay confirmed that compounds **32g** and **32h** showed promising selectivity profiles.

2.7. Inhibitory effect of cell growth, colony formation and gene expression in prostate cancer cells.

CBP and EP300 have been linked to the development of various diseases. CBP inhibitors have been evaluated for their therapeutic potential for the treatment of acute leukemia [28,39,40]. In this study, we tested our selective CBP inhibitors to determine if they possess any growth inhibition effects on prostate cancer cell lines. We selected AR-dependent prostate cancer cell lines such as LNCaP and 22Rv1 cells to test the cellular proliferation inhibition effects (Table 4). Enzalutamide, a second generation of AR antagonist, was chosen as positive control. The most potent compounds **32a**, **32g**, and **32h** did not show inhibition effect against LNCaP and 22Rv1 cells, which may be due to the highly polar carboxyl group found in **32a**, **32g** and **32h** restricting cellular permeability. Therefore, the polarity of the acid group was masked with ester [41,42]. In this case, the *tert*-butyl ester derivatives **29a**, **29g** and **29h** were obtained for corresponding carboxyl substituted compounds **32a**, **32g**, and **32h**. In the AlphaScreen assay, the esters derivatives **29a**, **29g** and **29h** were found to bind to CBP with IC_{50} values of 1.05, 1.04 and 0.42 μM, respectively. However, the esters derivatives **29a**, **29g** and **29h** showed reasonable potency in prostate cells LNCaP and 22Rv1, with IC_{50} values of approximately 2.0 μM (Figure 7A,B). These antiproliferative activities were appoximately 17-fold potent than that of the positive control enzalutamide (Table 4).

The antiproliferative activity of the compound **29h** was also evaluated against a wide range of cancer cell lines (Table S4). Not surprisingly, the compound did not show obvious inhibition on the growth of AR-negative prostate cancer cells PC-3 (IC_{50} > 20 μM). **29h** also displayed very weak inhibitory activities against breast cancer cell lines MCF-7 (ER positive), Hs578T (triple negative) and MDA-MB-231 (triple negative) with

IC_{50} value of 7.46, 15.09 and 35.99 μM, respectively. The growth inhibitory activities of the compound against lung fibroblast HFL-1 cells and human normal liver HL7702 cells were also evaluated to monitor the potential toxic effects. As show in Table S4, compound **29h** exhibited less cytotoxic effect against these two normal cells with IC_{50} values of 100 μM and 40 μM, respectively, indicating that the cytotoxic effects of **29h** was minimal.

To further investigate the growth inhibition effects, colony formation assays were performed for representative compounds **32g** and **32h** and their *tert*-butyl ester derivatives **29g** and **29h**. Similar to the cell viability assay, compounds **32g** and **32h** show no inhibitory activity for colony formation. However, the ester derivatives **29g** and **29h** reduced colony formation in a dose-dependent manner (Figure 7C,D). Colony formations were reduced to less than 10% in 22Rv1 and C4-2B cells at 4 μM. Thus, **29g** and **29h** significantly inhibit growth of prostate cancer cells. Overall, **32g**, **32h** and their ester derivatives **29g** and **29h** have good profiles for further optimization.

To investigate whether CBP inhibitors suppress the expression of full length AR, AR spliced variants, and AR-regulated target genes, qRT-PCR was performed in LNCaP cells. As shown in Figure 8A, compound **29h** strongly inhibited mRNA expression of full length AR. The AR-regulated genes KLK2, PSA (also known as KLK3) and TMPRSS2 were also inhibited upon **29h** treatment. Myc, a known oncogenic driver in prostate cancer, was also strongly inhibited by **29h**. Furthermore, western blot analysis indicated

that treatment of 22Rv1 cells with compound **29h** resulted in down regulation of AR-FL and AR-V7 level (Figure S2).

In a PSA luciferase reporter gene assay in LNCaP cells, both **29g** and **29h** significantly reduced the expression level of PSA in a dose-dependent manner (Figure 8B). These results indicated that targeting CBP may represent an alternative strategy for the treatment of CRPC.

3. Conclusions

In this study, we report the discovery of the 1-(1*H*-indol-1-yl)ethanone derivatives as CBP/EP300 bromodomain inhibitors for the treatment of CRPC through structure-based virtual screening, medicinal chemistry optimization, and biological evaluation. Determination of the high-resolution crystal structure of the inhibitor with the CBP provided guidance for structure-based optimization. The ester derivative **29h** potently inhibited cell growth or colony formation in the prostate cancer cell lines LNCaP, 22Rv1 and/or C4-2B. **29h** also reduced the expression of AR, c-Myc and AR target genes. Further optimization of **29h** may ultimately provide a new class of therapeutics for the treatment of CRPC.

4. Experimental section

4.1. Computational methods.

The crystal structure of CBP bromodomain (PDB ID: 4TS8.pdb) [34] was used for the molecular docking study. All of the ligand and protein preparation were performed with in Maestro (version 9.4, Schrödinger, LLC, New York, NY, 2013) implemented in the Schrödinger program (http://www. Schrödinger.com). The SPECS database (http://www.specs.net), containing more than 270,000 molecules, was filtrated with a molecular weight threshold of less than 300 Dalton. The resultant fragment dataset was submitted to molecular docking study. The molecular docking study was performed with the Glide program using the standard precision (SP) score mode. Top 5000 compounds were selected for cluster analysis and visual inspection. The molecules, which bear a carbon bond and form hydrogen bond with conserved Asn1168, were selected and submitted for subsequent biological evaluation.

4.2 General chemistry.

All commercial reagents and anhydrous solvents were purchased and used without purification, unless otherwise specified. Flash chromatography was performed using silica gel (300−400 mesh). All reactions were monitored by TLC, using silica gel plates with fluorescence F254 and UV light visualization. All products were characterized by their NMR and MS spectra. ^{1}H NMR spectra were recorded using a Bruker AV-400 spectrometer at 400 MHz or 500 MHz and ^{13}C NMR spectra were recorded using a Bruker AV-500 spectrometer at 500 MHz. Coupling constants (*J*) are expressed in hertz (Hz). Chemical shifts (δ), which relative to internal control (TMS), are reported in parts

per million (ppm) units. The low resolution of ESI-MS was recorded on an Agilent 1200 HPLC-MSD mass spectrometer. The purities of compounds were determined to be over 95% by reverse-phase high performance liquid chromatography (HPLC) analysis. HPLC instrument: Dionex Summit HPLC (column: Inertsil ODS-SP, 5.0 μm, 4.6 mm × 250 mm (GL Sciences Inc.); detector, UVD170U; injector, manual injector; pump, P680; detection wavelength, 254 nm; flow rate, 1.0 mL/min.

4.2.1 Procedure a of scheme 1.

A mixture of methyl piperidine-4-carboxylate (2 g, 14 mmol) (**20a**), 2-chloroacetyl chloride (1.16 mL, 15.4 mmol) and K_2CO_3 (5.8 g, 42 mmol) in DCM was stirred for 5 h at rt. Upon completion, the solvent was removed in vacuo. Water was added and the mixture was extracted with ethyl acetate (20 mL × 3). The organic layer was washed with water, 1 N HCl and brine, dried over Na_2SO_4, and evaporated. The compound **21a** (methyl piperidine-4-carboxylate) was obtained as a yellow oil (2.072 g, 67.4% yield). This oil was used in the next step without further purification. MS (APCI), m/z for $C_9H_{14}ClNO_3$ ($[M + H]^+$): Calcd 219.67, found 220.1.

4.2.2 Procedure b of scheme 1.

To a solution of compound **21a** (437.48 mg, 2 mmol) in acetone (50 mL) was added 1-(1*H*-indol-3-yl)ethanone (264 mg, 1.66 mmol), K_2CO_3 (688 mg, 4.98 mmol) and KI (42 mg, 0.252 mmol). The mixture was heated under reflux for 5 h. The aqueous layer was extracted with ethyl acetate (50 mL × 3), and the organic layer was washed with water and brine, dried over Na_2SO_4 and concentrated under reduced pressure. The residue

was purified by chromatography on silica gel to afford methyl 1-(2-(3-acetyl-1*H*-indol-1-yl)acetyl)piperidine-4-carboxylate (**22b**) (397 mg, 70% yield) as a white solid. ^{1}H NMR (400 MHz, DMSO-d_6) δ 8.24 (s, 1H), 8.18 (d, *J* = 6.9 Hz, 1H), 7.44 (d, *J* = 7.2 Hz, 1H), 7.20 (s, 2H), 5.29 (d, *J* = 4.7 Hz, 2H), 4.17 (d, *J* = 12.5 Hz, 1H), 3.94 (d, *J* = 12.9 Hz, 1H), 3.64 (s, 3H), 3.24 (t, *J* = 12.1 Hz, 1H), 2.80 (t, *J* = 11.7 Hz, 1H), 2.69 (t, *J* = 10.7 Hz, 1H), 2.42 (s, 3H), 1.94 (d, *J* = 11.6 Hz, 1H), 1.86 (d, *J* = 12.6 Hz, 1H), 1.71 (d, *J* = 10.5 Hz, 1H), 1.44 (d, *J* = 9.9 Hz, 1H). ^{13}C NMR (125 MHz, DMSO-d_6) δ 192.05, 174.28, 164.91, 138.48, 137.57, 125.49, 122.55, 121.73, 121.27, 115.98, 110.75, 51.50, 47.40, 43.48, 40.86, 28.02, 27.50, 27.16, 18.48. MS (APCI), m/z for $C_{19}H_{22}N_2O_4$ ($[M + H]^+$): Calcd 342.39, found 343.1. HPLC analysis: MeOH − H2O (80:20), 5.20 min, 99.68% purity. The synthesis of **22a** and **22c** can refer to **22b** (for details, see Supporting Information).

4.2.3 Procedure c of scheme 1.

Methyl 1-(2-(3-acetyl-1*H*-indol-1-yl)acetyl)piperidine-4-carboxylate (284 mg, 0.83 mmol) in a mixture of MeOH (8 mL) was treated with 1 N NaOH (4 mL, 4.15 mmol) and stirred for 2 h at room temperature. Then concentrated to remove MeOH and cooled to room temperature in an ice bath and neutralized with 1 N HCl. The solid precipitate was collected by filtration, washed with water and dried. 1-(2-(3-acetyl-1*H*-indol-1-yl)acetyl)piperidine-4-carboxylic acid (**22d**) (156 mg, 57.2% yield) was white solid. ^{1}H NMR (400 MHz, DMSO-d_6) δ 12.32 (s, 1H), 8.23 (s, 1H), 8.20 – 8.09 (m, 1H), 7.46 (dd, *J* = 21.2, 7.4 Hz, 1H), 7.27 – 7.14 (m, 2H), 5.36 – 5.22 (m, 2H), 4.16 (d, *J* = 13.0 Hz, 1H), 3.94 (d, *J* = 13.4 Hz, 1H), 3.27 – 3.19 (m, 1H), 2.81 (t, *J* = 11.1

Hz, 1H), 2.61 – 2.55 (m, 1H), 2.43 (s, 3H), 1.98 – 1.89 (m, 1H), 1.85 (d, *J* = 11.2 Hz, 1H), 1.69 (d, *J* = 10.6 Hz, 1H), 1.43 (d, *J* = 9.9 Hz, 1H), 1.24 (s, 1H). ^{13}C NMR (125 MHz, DMSO-d_6) δ 192.12, 175.49, 164.92, 138.58, 137.59, 125.50, 122.58, 121.75, 121.28, 115.97, 110.80, 47.45, 43.63, 41.02, 41.02, 27.18. MS (APCI), m/z for $C_{18}H_{20}N_2O_4$ ([M + H]$^+$): Calcd 328.36, found 329.1. HPLC analysis: MeOH (1‰ TFA) − H_2O (90:10), 4.15 min, 96.64% purity. The synthesis of **22e** can refer to **22d** (for details, see Supporting Information).

4.2.4 Procedure a of scheme 2.

1*H*-indole-3-carboxylic acid (**23a**) (1.5 g, 9.3 mmol), Et_3N (4 mL, 27.9 mmol) and DMAP (0.114 g, 0.93 mmol) were dissolved in DCE (12 mL). Then acetic anhydride (2.8 mL, 27.9 mmol) was added and the mixture was stirred for 2 h at 60 ºC. Upon completion, the solvent was evaporated. The residue was dissolved in EtOAc, extracted with saturated $NaHCO_3$ solution (20 mL × 3), the aqueous phase was cooled to 0 °C and then acidified with 1 N HCl. The precipitated solid was collected by filtration, washed with water and dried in vacuum to obtain the desired compound 1-acetyl-1*H*-indole-3-carboxylic acid (**24a**) (1.2 g, 63% yield) as white solid. ^{1}H NMR (400 MHz, DMSO-d_6) δ 8.42 (s, 1H), 8.35 (dd, *J* = 6.9, 1.8 Hz, 1H), 8.08 (dd, *J* = 6.5, 2.1 Hz, 1H), 7.44 – 7.28 (m, 2H), 2.73 (s, 3H).

4.2.5 Procedure b of scheme 2.

The *N*-(2-aminoethyl)acetamide (153 mg, 0.74mmol), HATU (218 mg, 0.74 mmol) and DIPEA (191 mg, 1.48 mmol) were dissolved in DCM. The mixture was stirred at rt for

30 min. The 1-acetyl-1*H*-indole-3-carboxylic acid (**24a**) (100 mg, 0.49 mmol) was then added, the reaction mixture was stirred overnight at rt. The aqueous layer was extracted with EtOAc (30 mL × 3), and the organic layer was washed with water and brine, dried with Na_2SO_4, and evaporated. The residue was purified by silica gel to yield *N*-(2-acetamidoethyl)-1-acetyl-1*H*-indole-3-carboxamide (**25a**) (100 mg, 71% yield) as white solid. ^{1}H NMR (400 MHz, $CDCl_3$) δ 8.51 – 8.43 (m, 1H), 8.12 – 8.05 (m, 1H), 8.02 (s, 1H), 7.46 – 7.37 (m, 2H), 7.17 (s, 1H), 6.34 (s, 1H), 3.64 (dd, *J* = 10.7, 5.0 Hz, 2H), 3.55 (dd, *J* = 10.9, 5.5 Hz, 2H), 2.70 (s, 3H), 2.03 (s, 3H). ^{13}C NMR (125 MHz, DMSO-d_6) δ 170.68, 170.39, 164.24, 135.96, 129.65, 129.04, 126.03, 124.87, 122.46, 116.61, 116.59, 39.42, 39.36, 24.70, 23.58. MS (APCI), m/z for $C_{15}H_{17}N_3O_3$ ($[M + H]^+$): Calcd 287.32, found 288.1. HPLC analysis: MeOH − H_2O (80:20), 5.26 min, 98.69% purity.

The synthesis of **25b** can refer to **25a** (for details, see Supporting Information).

4.2.6 Another procedure b of scheme 2.

The methyl 3-aminobenzoate (288 mg, 1.55 mmol), 1-acetyl-1*H*-indole-3-carboxylic acid (300 mg, 1.86 mmol) (**24a**), 3-chloro-1-iodo-2-methylpyridin-1-ium (950 mg, 3.72 mmol) and n-Bu_3N (1379 mg, 7.44 mmol) were dissolved in toluene. Under nitrogen, the reaction mixture was stirred overnight at 90 °C. It was concentrated and redissolved in EtOAc. The organic phase was extracted with saturated NH_4Cl solution, saturated $NaHCO_3$ solution, 1 N HCl and brine. The combined organic phase was dried over Na_2SO_4 and concentrated under reduced pressure. The resulting crude product was

purified by silica gel chromatography to yield methyl 3-(1-acetyl-1*H*-indole-3-carboxamido)benzoate (**25c**) (185 mg, 30% yield) as white solid. ^{1}H NMR (400 MHz, DMSO-d_6) δ 10.28 (s, 1H), 8.83 (s, 1H), 8.39 (s, 1H), 8.36 (s, 1H), 8.27 (d, *J* = 7.1 Hz, 1H), 8.14 (d, *J* = 7.9 Hz, 1H), 7.70 (d, *J* = 7.7 Hz, 1H), 7.54 (t, *J* = 7.9 Hz, 1H), 7.40 (dq, *J* = 13.8, 6.8 Hz, 2H), 3.89 (s, 3H), 2.76 (s, 3H). ^{13}C NMR (125 MHz, DMSO-d_6) δ 170.80, 167.04, 163.01, 140.40, 136.03, 131.02, 130.77, 130.16, 129.03, 126.31, 125.17, 125.15, 124.84, 122.46, 121.20, 116.73, 116.03, 53.11, 24.82. MS (APCI), m/z for $C_{19}H_{16}N_2O_4$ ($[M - H]^-$): Calcd 336.35, found 334.6. HPLC analysis: MeOH − H_2O (80:20), 10.71 min, 99.45% purity. The synthesis of **22d** can refer to **25c** (for details, see Supporting Information).

4.2.7 Procedure c of scheme 2.

Methyl 3-(1-acetyl-1*H*-indole-3-carboxamido)benzoate (**25c)** (100 mg, 0.3 mmol) in a mixture of MeOH (10 mL) was treated with 1 N NaOH (1.5 mL, 1.5 mmol) and stirred for overnight at room temperature. Then concentrated to remove MeOH and cooled to room temperature and acidified with 1N HCl. The solid was collected by filtration, rinsed with water and dried, the 3-(1*H*-indole-3-carboxamido)benzoic acid was obtained (**25e)**. ^{1}H NMR (400 MHz, DMSO-d_6) δ 12.91 (s, 1H), 11.75 (s, 1H), 9.89 (s, 1H), 8.39 (s, 1H), 8.34 (d, *J* = 3.0 Hz, 1H), 8.21 (d, *J* = 7.4 Hz, 1H), 8.07 (d, *J* = 8.1 Hz, 1H), 7.62 (d, *J* = 7.7 Hz, 1H), 7.47 (d, *J* = 7.3 Hz, 1H), 7.44 (d, *J* = 7.9 Hz, 1H), 7.26 – 7.08 (m, 2H).

4.2.8 Procedure d of scheme 2.

A mixture of 3-(1*H*-indole-3-carboxamido)benzoic acid (**26)** (67 mg, 0.23 mmol), Et_3N (68.68 mg, 0.68 mmol) and DMAP (2.8 mg, 0.023 mmol) in DCE (10 mL). Acetic anhydride (69.36 mL, 0.68 mmol) was added and stirred for 12 h at 60 ºC. Then concentrated to remove DCE and diluted with EtOAc, the organic phase was extracted with saturated $NaHCO_3$ solution, 1 N HCl and brine. The combined organic phases were dried over Na_2SO_4 and concentrated under reduced pressure. The expected compound 3-(1-acetyl-1*H*-indole-3-carboxamido)benzoic acid (**25e**) was obtained (26 mg, 35% yield) as white solid; ^{1}H NMR (400 MHz, DMSO-d_6) δ 12.99 (s, 1H), 10.24 (s, 1H), 8.84 (s, 1H), 8.37 (dd, *J* = 9.7, 1.5 Hz, 2H), 8.27 (dd, *J* = 6.5, 1.3 Hz, 1H), 8.11 (dd, *J* = 8.1, 1.1 Hz, 1H), 7.68 (d, *J* = 7.8 Hz, 1H), 7.51 (t, *J* = 7.9 Hz, 1H), 7.40 (pd, *J* = 7.2, 1.4 Hz, 2H), 2.76 (s, 3H). ^{13}C NMR (125 MHz, DMSO-d_6) δ 169.74, 167.09, 161.96, 139.21, 135.05, 131.30, 129.66, 128.86, 128.07, 125.26, 124.10, 123.85, 121.46, 120.59, 115.70, 115.18, 23.76. MS (APCI), m/z for $C_{18}H_{14}N_2O_4$ ($[M + H]^+$): Calcd 322.32, found 323.0. HPLC analysis: MeOH (1‰ TFA) − H_2O (90:10), 4.95 min, 99.12% purity.

4.2.9 Procedure a of scheme 3.

The synthesis of compound 1-acetyl-5-methoxy-1*H*-indole-3-carboxylic acid (**24b**) (38% yield) can refer to 1-acetyl-1*H*-indole-3-carboxylic acid (**24a**). The solid was white. ^{1}H NMR (400 MHz, DMSO-d_6) δ 8.39 (s, 1H), 8.24 (d, *J* = 9.1 Hz, 1H), 7.55 (d, *J* = 2.6 Hz, 1H), 7.00 (dd, *J* = 9.1, 2.6 Hz, 1H), 3.81 (s, 3H), 2.71 (s, 3H).

4.2.10 Procedure b of scheme 3.

The *tert*-butyl 3-amino-5-(furan-2-yl)benzoate (450 mg, 1.74 mmol), 1-acetyl-5-methoxy-1*H*-indole-3-carboxylic acid (485 mg, 2.08 mmol) (**24b**), 3-chloro-1-iodo-2-methylpyridin-1-ium (1.07 g, 4.17 mmol) and n-Bu_3N (1.54 g, 8.4 mmol) were dissolved in toluene. The reaction mixture was stirred under N_2 atmosphere for 16 h at 90 °C. Afterwards the solvent was evaporated, water was added and extracted with EtOAc (3 x 50 mL). The combined organic layer was dried over Na_2SO_4 and concentrated under reduced pressure. The residue was purified by silica gel chromatography to provide the desired compound *tert*-butyl 3-(1-acetyl-5-methoxy-1*H*-indole-3-carboxamido)-5-(furan-2-yl)benzoate (**29a**) (370 mg, 45.1%) as white solid. ^{1}H NMR (400 MHz, DMSO-d_6) δ 10.31 (s, 1H), 8.82 (s, 1H), 8.45 (s, 1H), 8.25 (d, *J* = 9.0 Hz, 1H), 8.19 (s, 1H), 7.92 (s, 1H), 7.84 (d, *J* = 1.2 Hz, 1H), 7.78 (d, *J* = 2.6 Hz, 1H), 7.01 (m, 2H), 6.66 (dd, *J* = 3.3, 1.8 Hz, 1H), 3.84 (s, 3H), 2.74 (s, 3H), 1.60 (s, 9H). HRMS (ESI) for $C_{27}H_{26}N_2O_6$ $[M + H]^+$, calcd: 474.1790, found: 475.1828.

27a−27l, **28a−28q**, **29b−29h** were prepared by the method similar to that of **29a** (for details, see Supporting Information).

4.2.11 Procedure c of scheme 3.

Tert-butyl 3-(1-acetyl-5-methoxy-1*H*-indole-3-carboxamido)-5-(furan-2-yl)benzoate (**29a**) (50 mg, 0.011 mmol) was dissolved in DCM (10 mL) and trifluoroacetic acid (1 mL). The mixture was stirred at rt for 5 h. The solvent was removed and the reside was recrystallized with petroleum/ethyl acetate to afford the desired compound

3-(1-acetyl-5-methoxy-1*H*-indole-3-carboxamido)-5-(furan-2-yl)benzoic acid (**32a**) (36 mg, 78.3% yield) as white solid. ^{1}H NMR (400 MHz, DMSO-d_6) δ 13.19 (s, 1H), 10.28 (s, 1H), 8.84 (s, 1H), 8.44 (s, 1H), 8.32 (s, 1H), 8.25 (d, *J* = 9.0 Hz, 1H), 7.98 (s, 1H), 7.83 (d, *J* = 1.2 Hz, 1H), 7.80 (d, *J* = 2.5 Hz, 1H), 7.06 (d, *J* = 3.3 Hz, 1H), 7.01 (dd, *J* = 9.0, 2.6 Hz, 1H), 6.65 (dd, *J* = 3.3, 1.8 Hz, 1H), 3.84 (s, 3H), 2.74 (s, 3H). ^{13}C NMR (125 MHz, DMSO-d_6) δ 169.63, 166.98, 162.36, 156.53, 152.11, 143.50, 140.03, 132.13, 131.10, 130.37, 129.74, 129.30, 119.37, 119.11, 118.17, 116.66, 114.73, 114.26, 112.37, 106.87, 103.76, 55.38, 23.66. MS (APCI), m/z for $C_{23}H_{18}N_2O_6$ ([M − H]$^-$): Calcd 418.41, found 416.3. HRMS (ESI) for $C_{23}H_{18}N_2O_6$ [M + H]$^+$, calcd: 418.1165, found: 419.1241. HPLC analysis: MeOH (1‰ TFA) − H_2O (90:10), 9.34 min, 99.09% purity.

Other 1-(1*H*-indol-3-yl)ethanone derivatives **30a−30l**, **31a−31q** and **32e−32h** were synthesized by using the procedure similar to that of **32a** (for details, see Supporting Information).

4.2.12 Procedure d of scheme 3.

To a stirred solution of *tert*-butyl 3-(1-acetyl-5-methoxy-1*H*-indole-3-carboxamido)-5-(furan-2-yl)benzoate (**29a**) (50 mg, 0.11 mmol) in dry DCM (20 mL), boron tribromide (70.15 mg, 0.28 mmol) was dropwise added at 0 °C. The reaction mixture was warmed to room temperature and stirred for 15 h. Then the reaction was quenched with water at 0 °C, followed by extraction with DCM (20 mL x 3). The combined extracts were dried over anhydrous $MgSO_4$. The solvent was evaporated in vacuo, and the resulting crude product was purified by recrystallization to provide 3-(1-acetyl-5-hydroxy-1*H*-indole-3-carboxamido)-5-(furan-2-yl)benzoic acid (**32b**) (26

mg, 60% yield) as white solid. ^{1}H NMR (500 MHz, DMSO-d_6) δ 13.15 (s, 1H), 10.25 (s, 1H), 9.40 (s, 1H), 8.78 (s, 1H), 8.45 (s, 1H), 8.29 (s, 1H), 8.15 (s, 1H), 7.97 (s, 1H), 7.83 (s, 1H), 7.67 (s, 1H), 7.04 (s, 1H), 6.86 (s, 1H), 6.65 (s, 1H), 2.72 (s, 3H). ^{13}C NMR (125 MHz, DMSO-d_6) δ 169.23, 166.79, 162.24, 154.36, 152.06, 143.31, 139.95, 132.02, 130.93, 129.95, 129.31, 128.87, 119.30, 118.17, 116.33, 114.67, 114.19, 112.16, 106.59, 106.34, 106.47, 23.45. MS (APCI), m/z for $C_{22}H_{16}N_2O_6$ ([M − H]$^-$): Calcd 404.38, found 403.1. HPLC analysis: MeOH (1‰ TFA) − H_2O (90:10), 4.73 min, 95.35% purity.

4.2.13 Procedure e of scheme 3.

A mixture of commercially available 3-(1-acetyl-5-hydroxy-1*H*-indole-3-carboxamido)-5-(furan-2-yl)benzoic acid (**32b**) (200 mg, 0.49 mmol), K_2CO_3 (202 mg, 1.47 mmol) and bromoethane (0.05 mL, 0.73 mmol) in acetone (20 mL) is stirred at 70 °C. After the reaction was completed, the reaction mixture was cooled to room temperature. The reaction mixture was extracted with EtOAc (50 mL × 2). The organic layer was washed with brine and dried over Na_2SO_4. The solid was filtered off, and the filtrate was concentrated under reduced pressure. The resulting crude product was purified by silica gel chromatography to afford 3-(1-acetyl-5-ethoxy-1*H*-indole-3-carboxamido)-5-(furan-2-yl)benzoic acid (**32c**) as white solid (80 mg, 37.9% yield). ^{1}H NMR (500 MHz, DMSO-d_6) δ 11.89 (s, 1H), 10.06 (s, 1H), 8.50 (s, 1H), 8.42 (d, J = 2.3 Hz, 1H), 8.31 (s, 1H), 7.92 (s, 2H), 7.83 (s, 1H), 7.49 (d, J = 8.7 Hz, 1H), 7.02 (d, J = 3.0 Hz, 1H), 6.96 (d, J = 8.6 Hz, 1H), 6.65 (s, 1H), 4.29 (t, J = 6.6 Hz, 2H), 2.29 (s, 3H), 1.01 (t, J = 7.4 Hz, 3H). ^{13}C NMR (125 MHz, DMSO-d_6) δ 169.88, 165.54, 163.33, 152.12, 145.20, 143.47, 140.79, 133.99, 131.10,

131.04, 130.25, 126.77, 118.90, 118.38, 118.14, 116.84, 113.46, 112.52, 112.32, 110.19, 106.77, 61.03, 20.88, 14.25. MS (APCI), m/z for $C_{24}H_{20}N_2O_6$ ([M − H]$^-$): Calcd 432.43, found 430.8. HPLC analysis: MeOH (1‰ TFA) − H_2O (90:10), 5.95 min, 97.54% purity.

Compound **32d** was synthesized through an analogous procedure to that used for the synthesis of **32c** (for details, see Supporting Information).

4.3. Biological evaluation.

4.3.1. Protein expression and purification.

The bromodomains were expressed as a His6-fusion protein with a TEV cleavage site between His6 and bromodomain using the pET24a expression vector (Novagen). cDNA encoding bromodomain of human BRD4(1) (residues N44-E168), EP300 (residues A1040-G1161), CBP (residues R1081-G1197), BRD9 (residues L14-Q134), PCAF (residues G715-D831), BAZ2B (residues S1858-S1972), TIF(1) (residues G896-E1014) and TAF1(1) (residues R1377-D1503) were synthesized by Genscript. BL21 (DE3) cells transformed with these expression plasmids were grown in LB broth at 25 °C to an OD_{600} of approximately 1.0 and then induced with 0.1 mM isopropyl-β-D-1-thiogalactopyranoside (IPTG) at 16 °C for 16 h. Cells were harvested by centrifugation (6000 g for 15 min at 4 °C, JLA 81000 rotor, on a Beckman Coulter Avanti J-20 XP centrifuge) and were frozen at −80 °C as pellets for storage. Cells were resuspended in extract buffer (50 mM HEPES, pH 7.5 at 25 °C, 500 mM NaCl, 5 mM imidazole, 5% glycerol, and 0.5 mM TCEP (Tris(2-carboxyethyl)phosphine hydrochloride)) and high-pressure homogenized using an JN3000 PLUS high pressure

homogenizer (JNBIO, Guangzhou, China) at 4 °C. The lysate was collected on ice and centrifuged at 12000 g for 40 min. The supernatant was loaded onto a 5 mL $NiSO_4$-loaded HisTrap HP column (Ni-NTA, GE Healthcare, NJ). The column was washed with 20 mL of extract buffer (50 mM HEPES, pH 7.5 at 25 °C, 500 mM NaCl, 50 mM imidazole). The protein was eluted with a 50−500 mM imidazole gradient in elute buffer with 50 mM HEPES, pH 7.5 at 25 °C, 500 mM NaCl, 500 mM imidazole. The protein was concentrated and further purified by a gel filtration column (HiLoad, Superdex 75, 16/60, GE Healthcare). The sample purity of each fraction was examined by SDS-PAGE, and the sample concentration was determined by Bradford assay. Purified proteins were concentrated and stored in the gel filtration buffer (10 mM Hepes pH 7.5 at 25 °C, 150 mM NaCl, 0.5 mM TCEP) and were used for crystallization or stored at −80 °C for AlphaScreen, TSA, or ITC assay.

4.3.2. AlphaScreen assay.

Interactions between bromodomain-containing proteins (BCP) and ligands were assessed by luminescence-based AlphaScreen technology (Perkin Elmer) as previously described in references [9,10,37] using a histidine detection kit from PerkinElmer (Norwalk, CT). All of the reactions contained bromodomain-containing protein bound to nickel acceptor beads (5 μg/mL) and biotinylated acetylated histone H4 peptide bound to streptavidin donor beads (5 μg/mL) in the presence or absence of the indicated amounts of control compound SGC-CBP30 (**4**), or candidate compounds. The C-terminal biotinylated tetra-acetylated histone peptide H4 (bH4KAc4) sequence was H-SGRGK(Ac)GGK(Ac)GLGK(Ac)GGAK(Ac)RHRK-Biotin-OH (synthesized by

Genscript). The experiments were conducted with various protein/peptide ratio as follows for sensitive signal: BRD4(1) : bH4KAc4 = 50 nM : 50 nM; CBP : bH4KAc4 = 150 nM : 50 nM; EP300 : bH4KAc4 = 150 nM : 50 nM; BRD9 : bH4KAc4 = 150 nM : 50 nM; ATAD2 : bH4KAc4 = 100 nM : 100 nM; BAZ2B : bH3K14Ac = 150 nM : 100 nM; TAF1 = 150 nM: 50 nM; TIF1 = 500 nM : 100 nM; PCAF = 150 nM : 50 nM. All reagents were diluted in the buffer (50 mM MOPS, pH 7.4, 50 mM NaF, 50 μM CHAPS, and 0.1 mg/mL bovine serum albumin) and allowed to equilibrate at room temperature prior to addition to low-volume 384-well plates (ProxiPlate-384 Plus, PerkinElmer, USA). Plates were foil sealed to protect from light, incubated at room temperature for 2.5 h and read on an EnSpire plate reader (PerkinElmer, USA). When excited by a laser beam of 680 nm, the donor beam emits singlet oxygen that activates thioxene derivatives in the acceptor beads, which releases photons of 520–620 nm as the binding signal. All experiments were carried out in triplicate on the same plate. The results were based on an average of three experiments with standard errors typically less than 10% of the measurements.

4.3.3. Thermal stability shift assay (TSA).

Thermal stability shift assays were carried out using the Bio-Rad CFX96 Real-Time PCR system. All reactions were buffered in 10 mM HEPES, pH 7.5, 150 mM NaCl at a final concentration of 10 μM proteins and 200 μM compounds. The 20 μL reaction mix was added to the wells of 96-well PCR plate. SYPRO Orange (ABI, Sigma) was added as a fluorescence probe at a dilution of 1:1000 and incubated with compounds on ice for 30 min. Total DMSO concentration was restricted to 1% or less. Excitation and emission

filters for the SYPRO Orange dye were set to 465 and 590 nm, respectively. The temperature was raised with a step of 0.3 °C per minute from 30 to 75 °C, and fluorescence readings were taken at each (0.3 °C) interval. All experiments were performed in triplicates. Melting temperatures (T_m) were calculated by fitting the sigmoidal melt curve to the Boltzmann equation using GraphPad Prism. ΔT_m is the difference in Tm values calculated for reactions with and without compounds.

4.3.4. Cell culture, cell viability and cell colony formation assays.

LNCaP, 22Rv1 and C4-2B prostate cancer cells were cultured in RPMI1640, plus 10% FBS; Cells were grown at 37 °C in 5% CO_2 incubators. For cell viability, cells were seeded in 384-well plates at 500−1000 cells per well (optimum density for growth) in a total volume of 20 μL of media. After 12 h, 10 μL chemical compounds with 2-fold serial dilution was added in a final volume of 30 μL of media each well with final concentration from 5 nM to 100 μM. The measurement was conducted 96 h after seeded, 25 μL of Cell-Titer GLO reagents (Promega) was added, and luminescence was measured on GLOMAX microplate luminometer (Promega), according to the manufacturer's instructions. The estimated *in vitro* half-maximal inhibitory concentration (IC_{50}) values were calculated using GraphPad Prism 6 software.

For colony formation assay, 1500 and 2000 cells per well were seeded in a 6-well plate for C4-2B and 22Rv1, respectively. Cells were cultured with vehicle or indicated concentrations of compounds for 14 days with 3 mL medium. When the cell colony grew visible, the medium was removed and the plates were washed with 2 mL PBS for one

time. The cell colonies were stained with 2.5% crystal violet (in MeOH) for 2 h. The plates were scanned with a HP scanner.

4.3.5. RNA isolation and quantitative real-time PCR.

LNCaP cells were seeded in RPMI containing 10% FBS in 12-well plates. Cells were treated with vehicle or **29h** (5 μM) for 48 hours. Total RNA was then isolated with the Eastep ® Super Total RNA Extraction Kit and cDNA was synthesized from 1,000 ng total RNA using the All-in-oneTM First-Strand cDNA Synthesis Kit. qPCRs were performed in triplicate using standard SYBR green reagents. Full length AR, AR-V7, PSA (KLK3), KLK2, TMPRSS2, MYC and ERG gene expression levels were assessed by real-time PCR, normalizing to the β-Actin. The primer sequences for qPCR used are as follows:

AR-FL_fwd, ACA TCA AGG AAC TCG ATC GTA TCA TTG C;

AR-FL_rev, TTG GGC ACT TGC ACA GAG AT;

PSA_fwd, CAC AGG CCA GGT ATT TCA GGT;

PSA_rev, GAG GCT CAT ATC GTA GAG CGG;

KLK2_fwd, CAA CAT CTG GAG GGG AAA GGG;

KLK2_rev, AGG CCA AGT GAT GCC AGA AC;

TMPRSS2_fwd, CAA GTG CTC CAA CTC TGG GAT;

TMPRSS2_rev, AAC ACA CCG ATT CTC GTC CTC;

C-MYC_fwd, GGC TCC TGG CAA AAG GTC A;

C-MYC_rev, CTG CGT AGT TGT GCT GAT GT;

β-Actin_fwd, GAG AAA ATC TGG CAC CAC ACC;

β-Actin_rev, ATA CCC CTC GTA GAT GGG CAC.

4.3.6. PSA luciferase reporter gene assay.

LNCaP cells were seeded in 24-well plates and transiently transfected using Lipofectamine 3000 (Invitrogen) according to the manufacturer's instructions. 200 ng PSA-Luc reporter plasmid and 10 ng renilla luciferase expression plasmid per well were cotransfected into LNCaP cells. Chemicals were added 24 h after transfection. The cells were harvested after another 24 h for a luciferase assay using the dual-luciferase reporter assay system (Promega). Luciferase activities were normalized to Renilla activity, which was co-transfected as an internal control. All of the assays were performed in triplicate, and the standard deviations were calculated accordingly.

4.3.7. Crystallization, data collection, and structure determination.

The purified and concentrated (10−15 mg/mL) CBP protein was incubated with ligands at a molar ratio of 1:3 for 40 min on ice. All crystallizations were carried out using the sitting drop vapor diffusion method in 24-well plate at 4 °C. Crystals of CBP with ligands were grown by mixing 1 μL of the protein (10−15 mg/mL) with 1 μL of reservoir solution containing various well buffers. Crystals of CBP with **22e** were grown with reservoir solution containing 0.2 M $MgCl_2$, 0.1 M Tris HCl, pH 8.5 and 30% PEG3350.

Crystals were cryoprotected using the well solution supplemented with additional ethylene glycol and were flash frozen in liquid nitrogen. All diffraction data were collected on beamlines BL18U1 at Shanghai Synchrotron Radiation Facilities (SSRF) at 100 K. Data sets were processed (indexing and integration) using the program MOSFLM

[43] and scaled using Aimless from the Collaborative Computational Project 4 (CCP4) program suite [44]. Molecular replacement was performed with the CCP4 program Phaser [45] using known CBP complex structure (PDB ID: 4NYX) as a search model. The model was refined using CCP4 program REFMAC5 [46] and rebuilt with COOT [47]. The quality of the models was checked using MolProbity [48]. Structure figures were prepared using the program PyMOL [49]. The statistics of data collection and the model refinement are summarized in Supporting Information, Table S3. Crystals of **22e** with CREBBP diffracted to resolutions of 1.62 Å.

Acknowledgements

We gratefully acknowledge financial support from the National Natural Science Foundation of China (grant 81373325, 81673357, 81400825 and 21602222), the International collaborative funds from Guangdong Province (2016A050502035), the "Personalized Medicines – Molecular Signature-based Drug Discovery and Development", Strategic Priority Research Program of the Chinese Academy of Sciences (grant No. XDA12020315), the Chinese National Programs for Key Research and Development (grant 2016YFB0201701), the Natural Science Foundation of Guangdong Province (2015A030312014), the Guangzhou Healthcare Collaborative Innovation Programs (201508020255). The authors thank the staffs from BL17U1, BL18U, BL19U1 beamlines of National Facility for Protein Science Shanghai (NFPS) at Shanghai Synchrotron Radiation Facility, for assistance during data collection. The authors gratefully acknowledge support from the Guangzhou Branch of the Supercomputing Center of Chinese Academy of Sciences.

Appendix A: Supplementary data

Supplementary date associated with this article can be found in the online version at http://dx.doi.org/xxxxxx. These data include MOL files and InChiKeys of the most important compounds described in this article, virtual screening results and primary biological evaluation, statistics of the data sets and structure refinement, chemistry part of synthesis and characterization.

References

[1] J. Ferlay, E. Steliarova-Foucher, J. Lortet-Tieulent, S. Rosso, J.W. Coebergh, H. Comber, D. Forman, F. Bray, Cancer incidence and mortality patterns in Europe: estimates for 40 countries in 2012, Eur J Cancer, 49 (2013) 1374-1403.

[2] R. Siegel, J. Ma, Z. Zou, A. Jemal, Cancer statistics, 2014, CA Cancer J Clin, 64 (2014) 9-29.

[3] I.A. Asangani, V.L. Dommeti, X. Wang, R. Malik, M. Cieslik, R. Yang, J. Escara-Wilke, K. Wilder-Romans, S. Dhanireddy, C. Engelke, M.K. Iyer, X. Jing, Y.M. Wu, X. Cao, Z.S. Qin, S. Wang, F.Y. Feng, A.M. Chinnaiyan, Therapeutic targeting of BET bromodomain proteins in castration-resistant prostate cancer, Nature, 510 (2014) 278-282.

[4] S.C. Chan, L.A. Selth, Y. Li, M.D. Nyquist, L. Miao, J.E. Bradner, G.V. Raj, W.D. Tilley, S.M. Dehm, Targeting chromatin binding regulation of constitutively active AR variants to overcome prostate cancer resistance to endocrine-based therapies, Nucleic Acids Res, 43 (2015) 5880-5897.

[5] A. Wyce, Y. Degenhardt, Y.C. Bai, B.C. Le, S. Korenchuk, M.C. Crouthamel, C.F. McHugh, R. Vessella, C.L. Creasy, P.J. Tummino, O. Barbash, Inhibition of BET bromodomain proteins as a therapeutic approach in prostate cancer, Oncotarget, 4 (2013) 2419-2429.

[6] R.J. Andersen, N.R. Mawji, J. Wang, G. Wang, S. Haile, J.K. Myung, K. Watt, T. Tam, Y.C. Yang, C.A. Banuelos, D.E. Williams, I.J. McEwan, Y.Z. Wang, M.D. Sadar, Regression of castrate-recurrent prostate cancer by a small-molecule inhibitor of the amino-terminus domain of the androgen receptor, Cancer Cell, 17 (2010) 535-546.

[7] L.J. Brand, M.E. Olson, P. Ravindranathan, H. Guo, A.M. Kempema, T.E. Andrews, X.L. Chen, G.V. Raj, D.A. Harki, S.M. Dehm, EPI-001 is a selective peroxisome proliferator-activated receptor-gamma modulator with inhibitory effects on androgen receptor expression and activity in prostate cancer, Oncotarget, 6 (2015) 3811-3824.

[8] J.K. Myung, C.A. Banuelos, J.G. Fernandez, N.R. Mawji, J. Wang, A.H. Tien, Y.C. Yang, I. Tavakoli, S. Haile, K. Watt, I.J. McEwan, S. Plymate, R.J. Andersen, M.D. Sadar, An androgen receptor N-terminal domain antagonist for treating prostate cancer, J Clin Invest, 123 (2013) 2948-2960.

[9] J. Wang, J.X. Zou, X. Xue, D. Cai, Y. Zhang, Z. Duan, Q. Xiang, J.C. Yang, M.C. Louie, A.D. Borowsky, A.C. Gao, C.P. Evans, K.S. Lam, J. Xu, H.J. Kung, R.M. Evans, Y. Xu, H.W. Chen, ROR-gamma drives androgen receptor expression and represents a therapeutic target in castration-resistant prostate cancer, Nat Med, 22 (2016) 488-496.

[10] Y. Zhang, X. Xue, X. Jin, Y. Song, J. Li, X. Luo, M. Song, W. Yan, H. Song, Y. Xu, Discovery of 2-oxo-1,2-dihydrobenzo[cd]indole-6-sulfonamide derivatives as

new RORgamma inhibitors using virtual screening, synthesis and biological evaluation, Eur J Med Chem, 78 (2014) 431-441.

[11] D. Chakravarti, V.J. LaMorte, M.C. Nelson, T. Nakajima, I.G. Schulman, H. Juguilon, M. Montminy, R.M. Evans, Role of CBP/P300 in nuclear receptor signalling, Nature, 383 (1996) 99-103.

[12] H.M. Chan, N.B. La Thangue, p300/CBP proteins: HATs for transcriptional bridges and scaffolds, J Cell Sci, 114 (2001) 2363-2373.

[13] K. Fronsdal, N. Engedal, T. Slagsvold, F. Saatcioglu, CREB binding protein is a coactivator for the androgen receptor and mediates cross-talk with AP-1, J Biol Chem, 273 (1998) 31853-31859.

[14] B. Hanstein, R. Eckner, J. DiRenzo, S. Halachmi, H. Liu, B. Searcy, R. Kurokawa, M. Brown, p300 is a component of an estrogen receptor coactivator complex, Proc Natl Acad Sci U S A, 93 (1996) 11540-11545.

[15] C. Missero, E. Calautti, R. Eckner, J. Chin, L.H. Tsai, D.M. Livingston, G.P. Dotto, Involvement of the cell-cycle inhibitor Cip1/WAF1 and the E1A-associated p300 protein in terminal differentiation, Proc Natl Acad Sci U S A, 92 (1995) 5451-5455.

[16] E.L. Chekler, J.A. Pellegrino, T.A. Lanz, R.A. Denny, A.C. Flick, J. Coe, J. Langille, A. Basak, S. Liu, I.A. Stock, P. Sahasrabudhe, P.D. Bonin, K. Lee, M.T. Pletcher, L.H. Jones, Transcriptional profiling of a selective CREB binding protein bromodomain inhibitor highlights therapeutic opportunities, Chem Biol, 22 (2015) 1588-1596.

[17] A.R. Conery, R.C. Centore, A. Neiss, P.J. Keller, S. Joshi, K.L. Spillane, P. Sandy, C. Hatton, E. Pardo, L. Zawadzke, A. Bommi-Reddy, K.E. Gascoigne, B.M. Bryant, J.A. Mertz, R.J. Sims, Bromodomain inhibition of the transcriptional coactivators CBP/EP300 as a therapeutic strategy to target the IRF4 network in multiple myeloma, Elife, 5 (2016) e10483.

[18] F. Faiola, X. Liu, S. Lo, S. Pan, K. Zhang, E. Lymar, A. Farina, E. Martinez, Dual regulation of c-Myc by p300 via acetylation-dependent control of Myc protein turnover and coactivation of Myc-induced transcription, Mol Cell Biol, 25 (2005) 10220-10234.

[19] S. Ghosh, A. Taylor, M. Chin, H.R. Huang, A.R. Conery, J.A. Mertz, A. Salmeron, P.J. Dakle, D. Mele, A. Cote, H. Jayaram, J.W. Setser, F. Poy, G. Hatzivassiliou, D. DeAlmeida-Nagata, P. Sandy, C. Hatton, F.A. Romero, E. Chiang, T. Reimer, T. Crawford, E. Pardo, V.G. Watson, V. Tsui, A.G. Cochran, L. Zawadzke, J.C. Harmange, J.E. Audia, B.M. Bryant, R.T. Cummings, S.R. Magnuson, J.L. Grogan, S.F. Bellon, B.K. Albrecht, R.J. Sims, J.M. Lora, Regulatory T cell modulation by CBP/EP300 bromodomain inhibition, J Biol Chem, 291 (2016) 13014-13027.

[20] D.A. Hay, O. Fedorov, S. Martin, D.C. Singleton, C. Tallant, C. Wells, S. Picaud, M. Philpott, O.P. Monteiro, C.M. Rogers, S.J. Conway, T.P. Rooney, A. Tumber,

C. Yapp, P. Filippakopoulos, M.E. Bunnage, S. Muller, S. Knapp, C.J. Schofield, P.E. Brennan, Discovery and optimization of small-molecule ligands for the CBP/p300 bromodomains, J Am Chem Soc, 136 (2014) 9308-9319.

[21] I. Ianculescu, D.Y. Wu, K.D. Siegmund, M.R. Stallcup, Selective roles for cAMP response element-binding protein binding protein and p300 protein as coregulators for androgen-regulated gene expression in advanced prostate cancer cells, J Biol Chem, 287 (2012) 4000-4013.

[22] N.G. Iyer, H. Ozdag, C. Caldas, p300/CBP and cancer, Oncogene, 23 (2004) 4225-4231.

[23] F. Wang, C.B. Marshall, M. Ikura, Transcriptional/epigenetic regulator CBP/p300 in tumorigenesis: structural and functional versatility in target recognition, Cell Mol Life Sci, 70 (2013) 3989-4008.

[24] J. Bouchal, F.R. Santer, P.P. Hoschele, E. Tomastikova, H. Neuwirt, Z. Culig, Transcriptional coactivators p300 and CBP stimulate estrogen receptor-beta signaling and regulate cellular events in prostate cancer, Prostate, 71 (2011) 431-437.

[25] Sachchidanand, L. Resnick-Silverman, S. Yan, S. Mutjaba, W.J. Liu, L. Zeng, J.J. Manfredi, M.M. Zhou, Target structure-based discovery of small molecules that block human p53 and CREB binding protein association, Chem Biol, 13 (2006) 81-90.

[26] T.D. Crawford, F.A. Romero, K.W. Lai, V. Tsui, A.M. Taylor, G.D. Boenig, C.L. Noland, J. Murray, J. Ly, E.F. Choo, T.L. Hunsaker, E.W. Chan, M. Merchant, S. Kharbanda, K.E. Gascoigne, S. Kaufman, M.H. Beresini, J.P. Liao, W.F. Liu, K.X. Chen, Z.G. Chen, A.R. Conery, A. Cote, H. Jayaram, Y. Jiang, J.R. Kiefer, T. Kleinheinz, Y.J. Li, J. Maher, E. Pardo, F. Poy, K.L. Spillane, F. Wang, J. Wang, X.C. Wei, Z.W. Xu, Z.Y. Xu, I. Yen, L. Zawadzke, X.Y. Zhu, S. Bellon, R. Cummings, A.G. Cochran, B.K. Albrecht, S. Magnuson, Discovery of a potent and selective in vivo probe (GNE-272) for the bromodomains of CBP/EP300, J Med Chem, 59 (2016) 10549-10563.

[27] O. Fedorov, H. Lingard, C. Wells, O.P. Monteiro, S. Picaud, T. Keates, C. Yapp, M. Philpott, S.J. Martin, I. Felletar, B.D. Marsden, P. Filippakopoulos, S. Muller, S. Knapp, P.E. Brennan, [1,2,4]triazolo[4,3-a]phthalazines: inhibitors of diverse bromodomains, J Med Chem, 57 (2014) 462-476.

[28] S. Picaud, O. Fedorov, A. Thanasopoulou, K. Leonards, K. Jones, J. Meier, H. Olzscha, O. Monteiro, S. Martin, M. Philpott, A. Tumber, P. Filippakopoulos, C. Yapp, C. Wells, K.H. Che, A. Bannister, S. Robson, U. Kumar, N. Parr, K. Lee, D. Lugo, P. Jeffrey, S. Taylor, M.L. Vecellio, C. Bountra, P.E. Brennan, A. O'Mahony, S. Velichko, S. Muller, D. Hay, D.L. Daniels, M. Urh, N.B. La Thangue, T. Kouzarides, R. Prinjha, J. Schwaller, S. Knapp, Generation of a selective small molecule inhibitor of the CBP/p300 bromodomain for leukemia therapy, Cancer Res, 75 (2015) 5106-5119.

[29] T.A. Popp, C. Tallant, C. Rogers, O. Fedorov, P.E. Brennan, S. Muller, S. Knapp, F. Bracher, Development of selective CBP/P300 benzoxazepine bromodomain inhibitors, J Med Chem, 59 (2016) 8889-8912.

[30] T.P. Rooney, P. Filippakopoulos, O. Fedorov, S. Picaud, W.A. Cortopassi, D.A. Hay, S. Martin, A. Tumber, C.M. Rogers, M. Philpott, M. Wang, A.L. Thompson, T.D. Heightman, D.C. Pryde, A. Cook, R.S. Paton, S. Muller, S. Knapp, P.E. Brennan, S.J. Conway, A series of potent CREBBP bromodomain ligands reveals an induced-fit pocket stabilized by a cation-pi interaction, Angew Chem Int Ed Engl, 53 (2014) 6126-6130.

[31] K. Shirakawa, L. Wang, N. Man, J. Maksimoska, A.W. Sorum, H.W. Lim, I.S. Lee, T. Shimazu, J.C. Newman, S. Schroder, M. Ott, R. Marmorstein, J. Meier, S. Nimer, E. Verdin, Salicylate, diflunisal and their metabolites inhibit CBP/p300 and exhibit anticancer activity, Elife, 5 (2016) e11156.

[32] A.M. Taylor, A. Cote, M.C. Hewitt, R. Pastor, Y. Leblanc, C.G. Nasveschuk, F.A. Romero, T.D. Crawford, N. Cantone, H. Jayaram, J. Setser, J. Murray, M.H. Beresini, G.D. Boenig, Z.G. Chen, A.R. Conery, R.T. Cummings, L.A. Dakin, E.M. Flynn, O.W. Huang, S. Kaufman, P.J. Keller, J.R. Kiefer, T. Lai, Y.J. Li, J.P. Liao, W.F. Liu, H. Lu, E. Pardo, V. Tsui, J. Wang, Y.Y. Wang, Z.W. Xu, F. Yan, D. Yu, L. Zawadzke, X.Q. Zhu, X.Y. Zhu, R.J. Sims, A.G. Cochran, S. Bellon, J.E. Audia, S. Magnuson, B.K. Albrecht, Fragment-based discovery of a selective and cell-active benzodiazepinone CBP/EP300 bromodomain inhibitor (CPI-637), Acs Medicinal Chemistry Letters, 7 (2016) 531-536.

[33] A. Unzue, M. Xu, J. Dong, L. Wiedmer, D. Spiliotopoulos, A. Caflisch, C. Nevado, Fragment-based design of selective nanomolar ligands of the CREBBP bromodomain, J Med Chem, 59 (2016) 1350-1356.

[34] A. Unzue, H.T. Zhao, G. Lolli, J. Dong, J. Zhu, M. Zechner, A. Dolbois, A. Caflisch, C. Nevado, The "Gatekeeper" residue influences the mode of binding of acetyl indoles to bromodomains, J Med Chem, 59 (2016) 3087-3097.

[35] M. Xu, A. Unzue, J. Dong, D. Spiliotopoulos, C. Nevado, A. Caflisch, Discovery of CREBBP bromodomain inhibitors by high-throughput docking and hit optimization guided by molecular dynamics, J Med Chem, 59 (2016) 1340-1349.

[36] Y. Song, X. Xue, X. Wu, R. Wang, Y. Xing, W. Yan, Y. Zhou, C.N. Qian, Y. Zhang, Y. Xu, Identification of N-phenyl-2-(N-phenylphenylsulfonamido)acetamides as new RORgamma inverse agonists: Virtual screening, structure-based optimization, and biological evaluation, Eur J Med Chem, 116 (2016) 13-26.

[37] X. Xue, Y. Zhang, Z. Liu, M. Song, Y. Xing, Q. Xiang, Z. Wang, Z. Tu, Y. Zhou, K. Ding, Y. Xu, Discovery of benzo[cd]indol-2(1H)-ones as potent and specific BET bromodomain inhibitors: structure-based virtual screening, optimization, and biological evaluation, J Med Chem, 59 (2016) 1565-1579.

[38] Y. Zhou, T. Nie, Y. Zhang, M. Song, K. Li, M. Ding, K. Ding, D. Wu, Y. Xu, The

discovery of novel and selective fatty acid binding protein 4 inhibitors by virtual screening and biological evaluation, Bioorg Med Chem, 24 (2016) 4310-4317.

[39] E.J. Gang, Y.T. Hsieh, J. Pham, Y. Zhao, C. Nguyen, S. Huantes, E. Park, K. Naing, L. Klemm, S. Swaminathan, E.M. Conway, L.M. Pelus, J. Crispino, C.G. Mullighan, M. McMillan, M. Muschen, M. Kahn, Y.M. Kim, Small-molecule inhibition of CBP/catenin interactions eliminates drug-resistant clones in acute lymphoblastic leukemia, Oncogene, 33 (2014) 2169-2178.

[40] B.E. Zucconi, B. Luef, W. Xu, R.A. Henry, I.M. Nodelman, G.D. Bowman, A.J. Andrews, P.A. Cole, Modulation of p300/CBP acetylation of nucleosomes by bromodomain ligand I-CBP112, Biochemistry (Mosc), 55 (2016) 3727-3734.

[41] M. Barot, M. Bagui, M.R. Gokulgandhi, A.K. Mitra, Prodrug strategies in ocular drug delivery, Med Chem, 8 (2012) 753-768.

[42] K.M. Huttunen, H. Raunio, J. Rautio, Prodrugs--from serendipity to rational design, Pharmacol Rev, 63 (2011) 750-771.

[43] A.G. Leslie, H.R. Powell, Processging diffraction data with mosflm., Evol Dev, 245 (2007) 41-51.

[44] Collaborative Computational Project, The CCP4 suite: programs for protein crystallography., Acta Crystallogr D Biol Crystallogr, 50 (2007) 760-763.

[45] A.J. McCoy, R.W. Grosse-Kunstleve, P.D. Adams, M.D. Winn, L.C. Storoni, R.J. Read, Phaser crystallographic software, Journal of applied crystallography, 40 (2007) 658-674.

[46] G.N. Murshudov, P. Skubak, A.A. Lebedev, N.S. Pannu, R.A. Steiner, R.A. Nicholls, M.D. Winn, F. Long, A.A. Vagin, REFMAC5 for the refinement of macromolecular crystal structures, Acta Crystallogr D Biol Crystallogr, 67 (2011) 355-367.

[47] P. Emsley, K. Cowtan, Coot: model-building tools for molecular graphics, Acta Crystallogr D Biol Crystallogr, 60 (2004) 2126-2132.

[48] V.B. Chen, W.B. Arendall, 3rd, J.J. Headd, D.A. Keedy, R.M. Immormino, G.J. Kapral, L.W. Murray, J.S. Richardson, D.C. Richardson, MolProbity: all-atom structure validation for macromolecular crystallography, Acta Crystallogr D Biol Crystallogr, 66 (2010) 12-21.

[49] DeLano, W. L. The PyMOL molecular graphics system. Palo Alto, CA: DeLano Scientific LLC, (2002)

Figure Legends

Figure 1. Structures of representative CBP bromodomain inhibitors. IC_{50} values for the inhibitors are shown with the method used.

Figure 2. Virtual screening and experimental validation for CBP bromodomain inhibitors. (A) The flowchart of virtual screening for CBP bromodomain inhibitors. (B) The inhibition rate of all tested compounds (**4** (SGC−CBP30) was used as positive control). (C) The inhibitory curves of **6** and **7**.

Figure 3. Predicted binding modes of **6** (A) and **7** (B) in complex with CBP protein. The ligands and important residues are shown as sticks. Water molecules are shown as red spheres. The hydrogen bonds are shown as yellow dashed lines. Figures were prepared using PyMOL.

Figure 4. Complex structures from co-crystal or prediction for compounds **22e** and **25e**. (A) Co-crystal structure of compound **22e** with CBP (PDB ID: 5XXH). (B) The omit F_o-F_c electron density map for compound **22e** shown as grid contoured at 3σ. (C) Predicted binding mode of **25e** in complex with CBP protein. The ligands are shown as sticks. The electrostatic potential surfaces are shown in transparent for clarity. The binding site residues are shown as lines. Hydrogen bonds interactions are indicated by dashed lines in yellow. Compounds are well-defined by the electron density.

Figure 5. Predicted binding modes for compounds **30l** (A), **31o** (B), **32g** (C), and **32h** (D). The ligands are shown as sticks, the binding site residues are shown as lines. The

electrostatic potential surfaces are shown in transparent for clarity. The water molecules are shown as sphere in red. Hydrogen bonds interactions are indicated by dashed lines in yellow.

Figure 6. Compounds **32g** and **32h** are selective CBP inhibitors. The bromodomains selectivity profiles were determined by thermal shift assay. Compound concentration, 200 μM; protein concentration, 10 μM. Heat map shows the relative ΔT_m values. Red indicates large ΔT_m, and green indicates small ΔT_m.

Figure 7. Growth inhibition effects of CBP inhibitors in different prostate cancer cell lines. (A) IC_{50} curves of **29a**, **29g** and **29h** toward the LNCaP cell line. (B) IC_{50} curves of **29a**, **29g** and **29h** toward the 22Rv1 cell line. (C) Compound **29g** inhibits C4-2B and 22Rv1 cancer cell colony formation. (D) Compound **29h** inhibits C4-2B and 22Rv1 cancer cell colony formation.

Figure 8. (A) qRT–PCR analysis for mRNA expression of AR and AR-related genes in LNCaP cells treated with vehicle (DMSO) or with **29h** (1 or 5 μM) for 48 h. (B) LNCaP cells were transfected with PSA-luc and treated with vehicle or with 0.4, 2.0 or 10 μM of **29g** and **29h**. Cells were lysed and assayed for luciferase activity. Data are expressed as the mean ± s.e.m. (n = 3). NS, not significant. *$p < 0.05$, **$p < 0.01$.

Table 1. **Structure-activity relationship studies of the LPF shelf.**

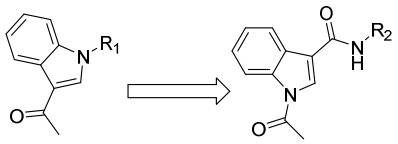

No.	R_1	R_2	AlphaScreen (μM)[a]	cLogP[b]	LE[c]
4	–	–	0.08	4.420	0.33
6	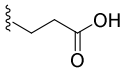	–	16.73	1.829	0.39
22a	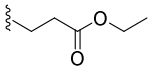	–	39.55±0.89	2.82	0.32
22b	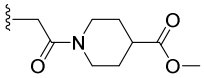	–	19.84±0.71	1.34	0.26
22c	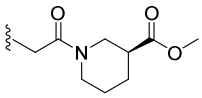	–	7.09±0.41	2.50	0.29
22d	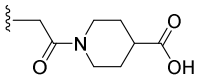	–	13.62±0.23	0.96	0.28
22e	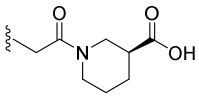	–	6.80±1.53	2.04	0.30
25a	–	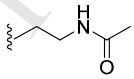	33.85±4.89	0.51	0.30
25b	–	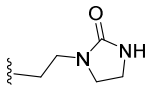	32.64±4.10	0.58	0.27
25c	–	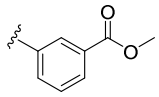	3.39±0.29	3.33	0.31
25d	–	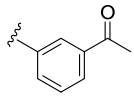	25.37±1.50	2.80	0.27
25e	–	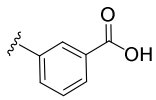	1.69±0.17	2.93	0.34

[a]The IC_{50} was calculated from the AlphaScreen assay. The data were expressed as the means ± SD, representing the data from at least two independent experiments. [b]cLogP values were calculated using ChemBiodraw Ultra12.0. [c]LE (Ligand Efficiency) = 1.4 (pIC_{50}/heavy atoms).

Table 2. **Structure-activity relationship studies of the ZA and BC channels.**

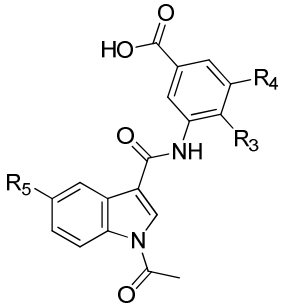

No.	R_3	R_4	R_5	AlphaScreen[a] (μM)
30a	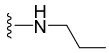	-H	-H	6.56±0.74
30b	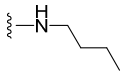	-H	-H	>50
30c	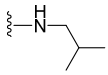	-H	-H	2.33±0.35
30d		-H	-H	4.84±0.37
30e	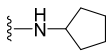	-H	-H	1.89±0.03
30f	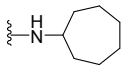	-H	-H	1.67±0.03
30g	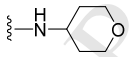	-H	-H	8.50±0.03
30h	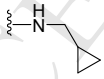	-H	-H	21.58±3.96
30i	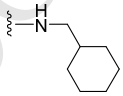	-H	-H	2.33±0.91
30j	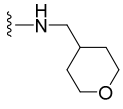	-H	-H	6.36±0.57
30k	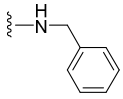	-H	-H	4.11±1.42
30l	-F	-H	-H	0.77±0.20

31a	-H	-Br	-H	4.70±0.19
31b	-H		-H	2.8±0.24
31c	-H		-H	3.39±0.93
31d	-H		-H	2.74±0.32
31e	-H		-H	2.99±0.38
31f	-H		-H	2.48±0.38
31g	-H	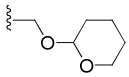	-H	1.00±0.27
31h	-H	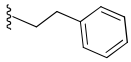	-H	1.96±0.13
31i	-H		-H	1.86±0.12
31j	-H		-H	3.52±0.18
31k	-H		-H	1.44±0.11
31l	-H	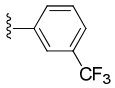	-H	4.05±0.13
31m	-H	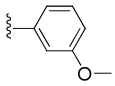	-H	2.07±0.03
31n	-H		-H	1.69±0.44
31o	-H		-H	0.65±0.06
31p	-H	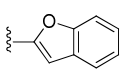	-H	2.81±0.35
31q	-H	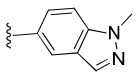	-H	1.00±0.11

32a	-H		-OMe	0.14±0.01
32b	-H		-OH	0.17±0.04
32c	-H		-OEt	3.89±0.56
32d	-H		-OPr	26.19±2.98
32e	-H	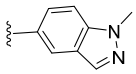	-OMe	0.29±0.06
32f	-H	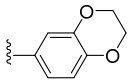	-OMe	0.69±0.09
32g	-H	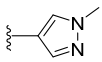	-OMe	0.16±0.01
32h	-F	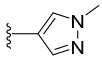	-OMe	0.037±0.01

[a]The IC_{50} was calculated from the AlphaScreen assay. The data were expressed as the means ± SD, representing the data from at least two independent experiments.

Table 3. 1-(1*H*-indol-1-yl)ethanone derivatives are selective CBP inhibitors.

No.	CBP	EP300	BRD4(1)	TAF1	BAZ2B	BRD9	TIF1	PCAF
4	0.08	0.23	> 20	> 20	> 20	> 20	> 20	> 20
25e	1.69	5.55	> 20	> 20	> 20	> 20	> 20	> 20
30l	0.77	4.45	> 20	> 20	> 20	> 20	> 20	> 20
31g	1.00	2.51	> 20	> 20	> 20	> 20	> 20	> 20
31o	0.65	0.97	2.19	> 20	1.69	> 20	10.44	> 20
32a	0.14	1.78	>20	> 20	12.16	> 20	> 20	> 20
32g	0.16	0.51	> 20	> 20	> 20	> 20	> 20	> 20
32h	0.046	0.049	> 20	> 20	> 20	> 20	> 20	> 20

The bromodomains selectivity profiles were determined by AlphaScreen. All IC_{50} values are reported as means of values from at least two determinations.

Table 4. Anti-proliferation effects against cell lines LNCaP and 22Rv1.

No.	IC_{50} (μM)	
	LNCaP[a]	22Rv1[b]
Enzalutamide[c]	33.84	36.66
4	NA	NA
32a	NA	NA
32g	NA	NA
32h	NA	NA
29a	1.76 ± 0.70	4.31
29g	1.28 ± 0.01	2.22
29h	2.01 ± 0.63	2.13

The IC_{50} was calculated from cell viability assay by Cell-Titer GLO (Promega). [a]The data were expressed as the means ± SD, representing at least two independent experiments. [b]This data was expressed from single experiment. [c]Enzalutamide is AR antagonist which was used as standard drug for prostate cancer.

Figure 1

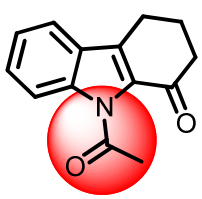

1 (MS7972)

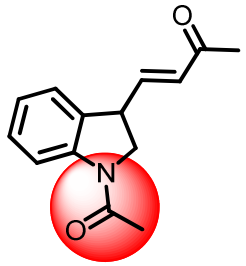

2 (MS7867)

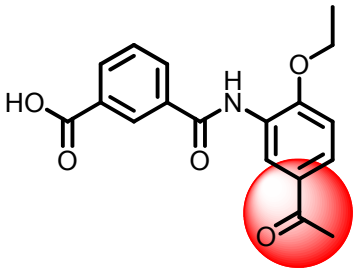

3

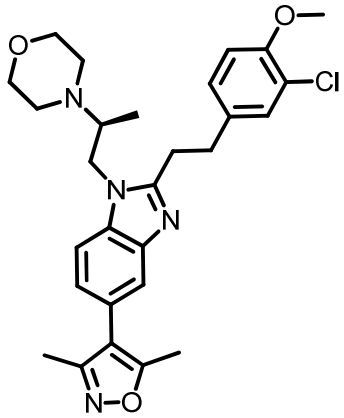

4 (SGC-CBP30)

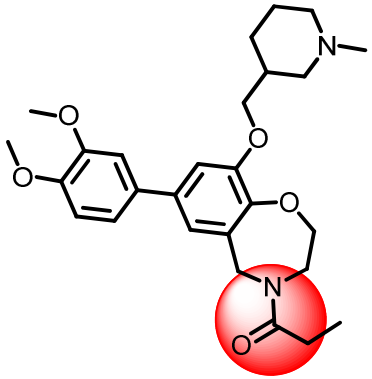

5 (I-CBP112)

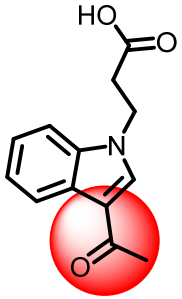

6

Figure 2

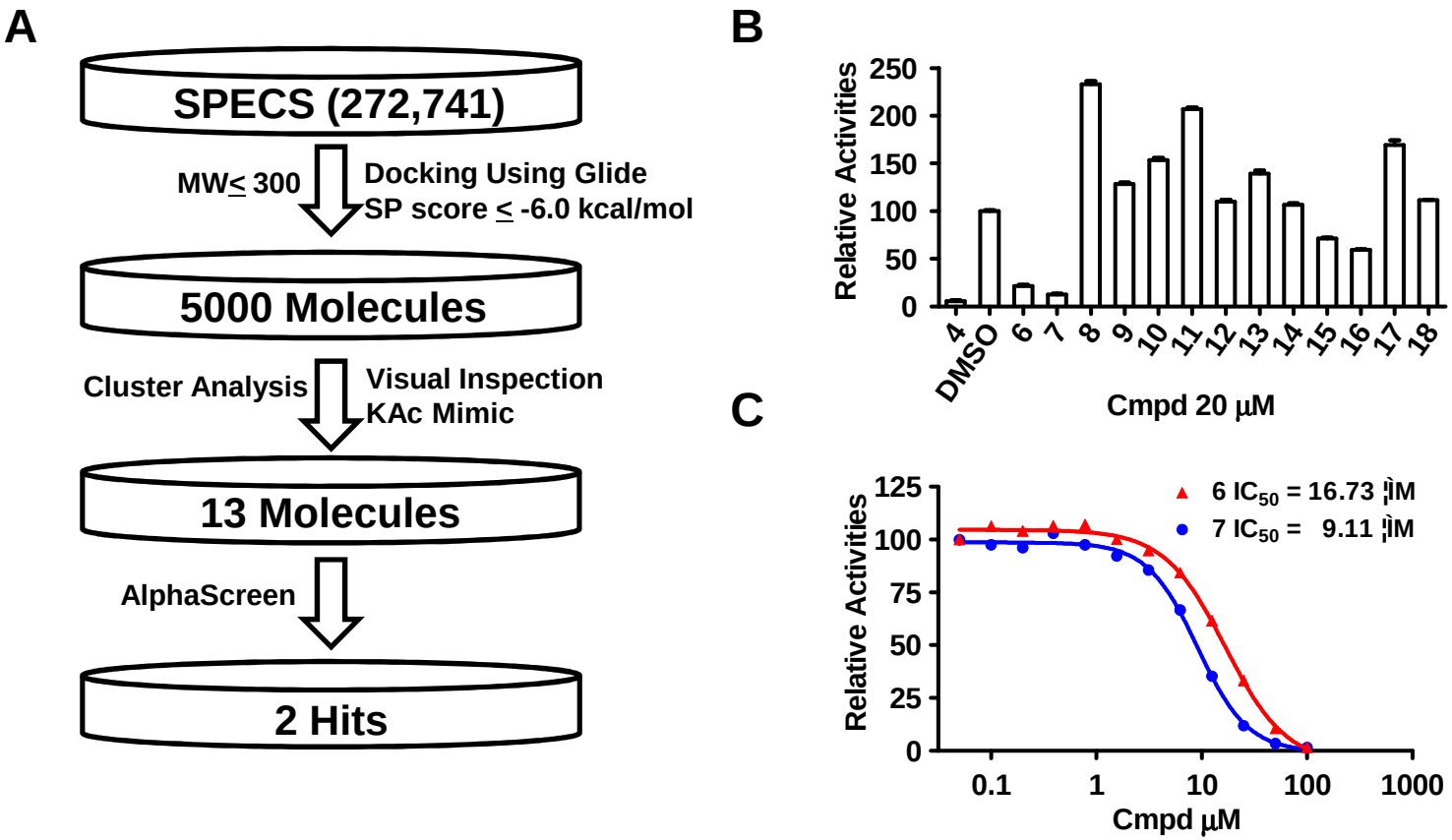

Figure 3

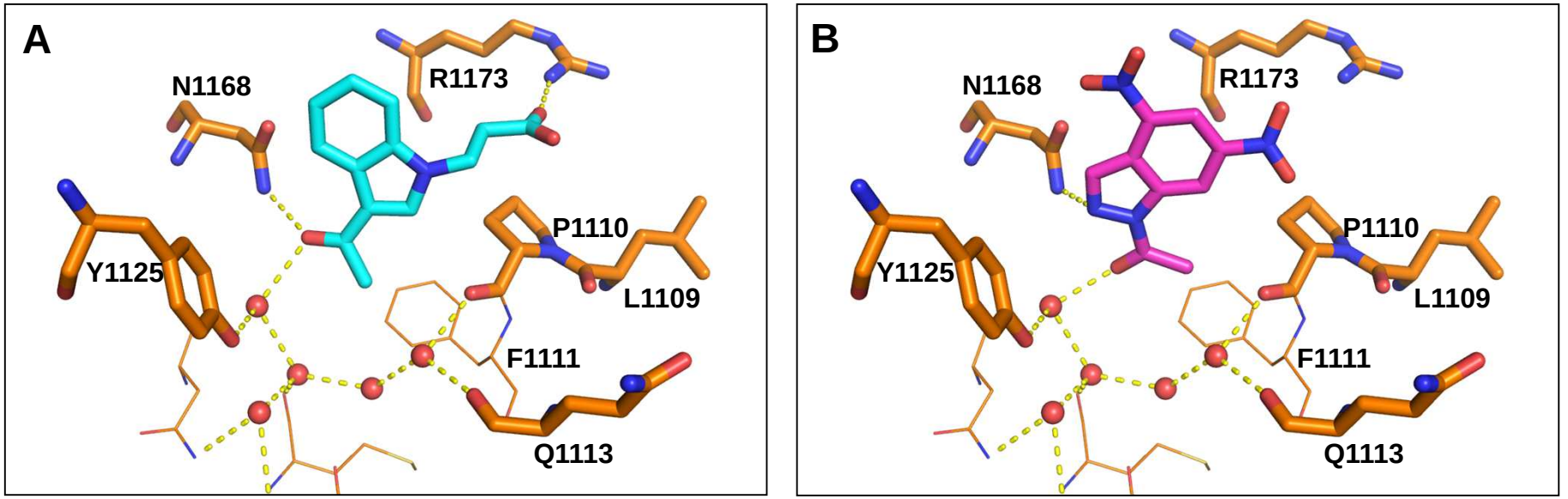

Figure 4

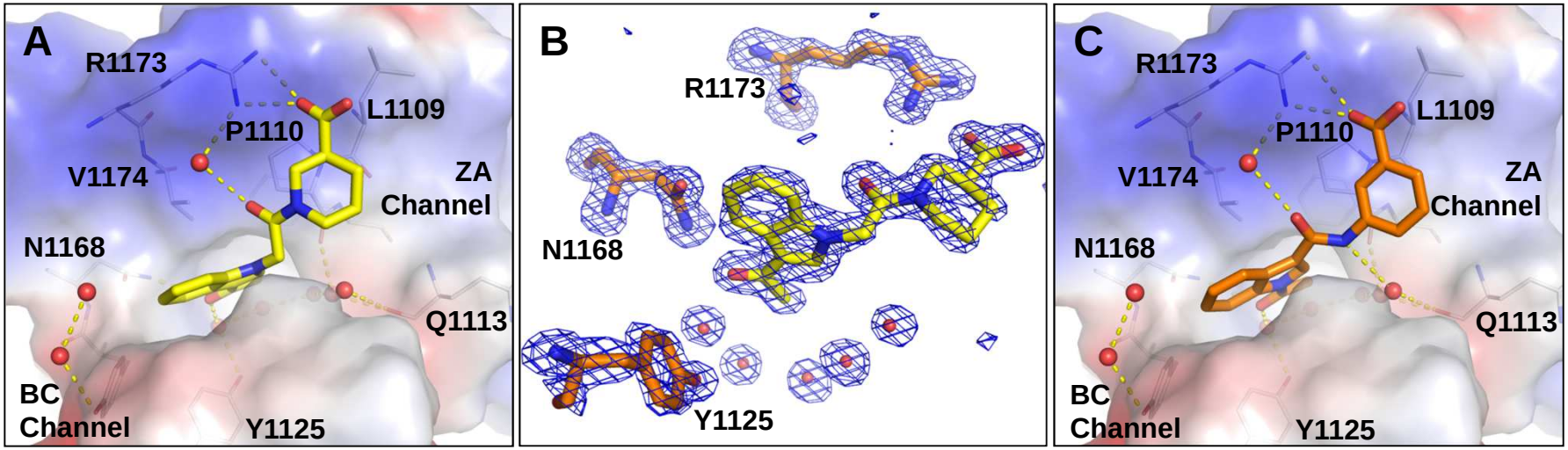
A
R1173
L1109
P1110
V1174
ZA
Channel
N1168
Q1113
BC
Channel
Y1125
B
R1173
N1168
Y1125
C
R1173
L1109
P1110
V1174
ZA
Channel
N1168
Q1113
BC
Channel
Y1125

Figure 5

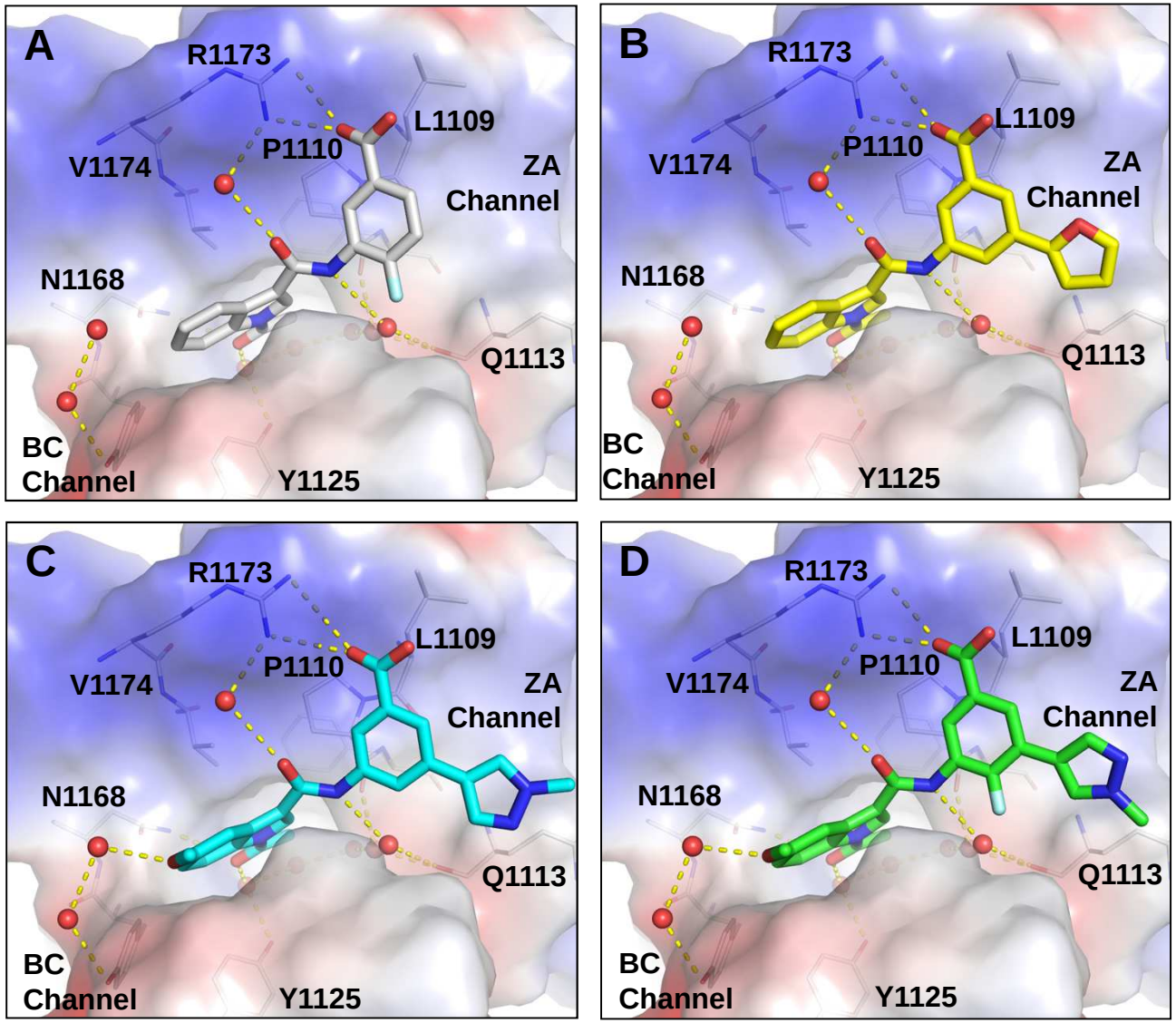
A
R1173
L1109
P1110
V1174
ZA
Channel
N1168
Q1113
BC
Channel
Y1125
B
R1173
L1109
P1110
V1174
ZA
Channel
N1168
Q1113
BC
Channel
Y1125
C
R1173
L1109
P1110
V1174
ZA
Channel
N1168
Q1113
BC
Channel
Y1125
D
R1173
L1109
P1110
V1174
ZA
Channel
N1168
Q1113
BC
Channel
Y1125

Figure 6

Cmpd/Protein	CBP	EP300	PCAF	BRD9	TAF1	BAZ2B	TIF1	BRD4
32g	5.7	5.7	-1.5	-0.9	0.9	1.5	-0.3	1.1
32h	8.7	7.2	-0.3	0.9	0.6	0.3	0	1.2

Figure 7

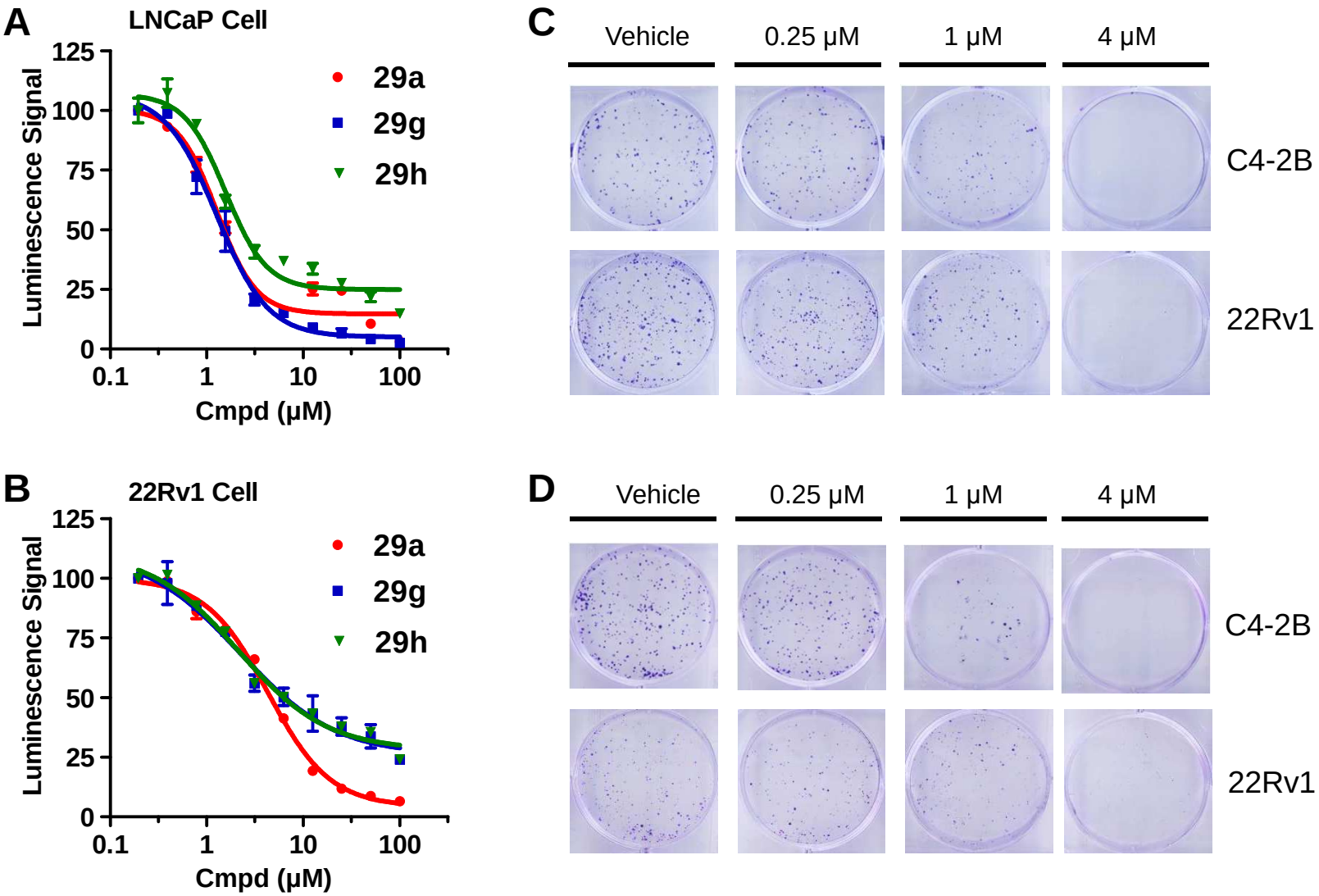
A
LNCaP Cell
Luminescence Signal
125
100
75
50
25
0
0.1
1
10
100
Cmpd (μM)
29a
29g
29h
B
22Rv1 Cell
Luminescence Signal
125
100
75
50
25
0
0.1
1
10
100
Cmpd (μM)
29a
29g
29h
C
Vehicle
0.25 μM
1 μM
4 μM
C4-2B
22Rv1
D
Vehicle
0.25 μM
1 μM
4 μM
C4-2B
22Rv1

Figure 8

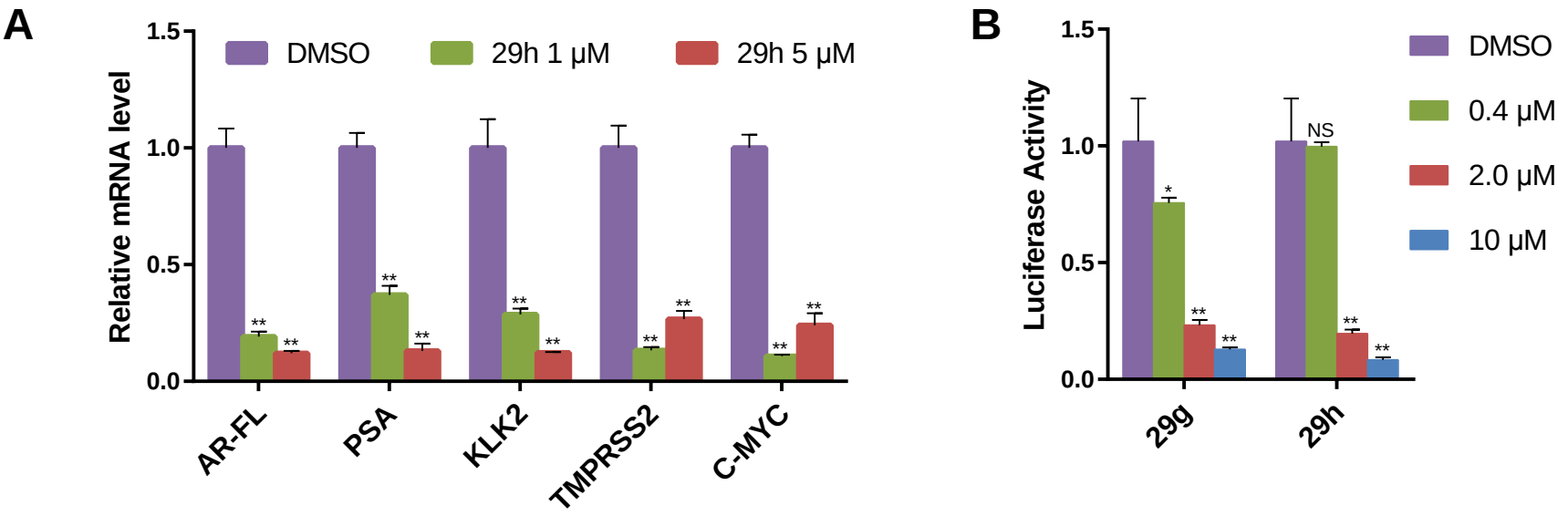
A
Relative mRNA level
1.5
1.0
0.5
0.0
DMSO
29h 1 μM
29h 5 μM
**
AR-FL
PSA
KLK2
TMPRSS2
C-MYC
B
Luciferase Activity
*
NS
29g
29h
DMSO
0.4 μM
2.0 μM
10 μM

Highlights:

Fragment-based virtual screening and optimization yielded selective CBP BRD inhibitors

CBP inhibitors potently suppress the expression of AR, AR-V7 in prostate cancer cells

CBP inhibitors markedly inhibit the growth and colony formation of prostate cancer cells

Targeting CBP represents a promising and alternative strategy for treatment of CRPC